Bactericidal activity of ZnO nanoparticles-anti TB drugs combination towards H37Rv strain and multidrug-resistant isolates of *Mycobacterium tuberculosis* via SufB splicing inhibition

Deepak Kumar Ojha[1], Ashwaria Mehra[1], Sunil Swick Rout[1], Sidhartha Giri[2] and Sasmita Nayak[1]*

[1]School of Biotechnology, Kalinga Institute of Industrial Technology Deemed to be University (KIIT-DU), Bhubaneswar, Odisha 751024, India

[2]National Reference Laboratory for Tuberculosis, ICMR-Regional Medical Research Centre (RMRC), Bhubaneswar, Odisha, 751023, India

*Corresponding Author: Dr. Sasmita Nayak, Email Id: sasmita.n@kiitbiotech.ac.in.

Abstract

Tuberculosis (TB) remains a significant global health threat, claiming millions of lives annually. Despite advancements in treatment, the emergence of drug-resistant strains has hindered effective TB control. The current management for TB is prolonged with severe side effects, leading to poor patient compliance. Metal-based nanoparticles are shown to manage drug-sensitive TB when combined with anti-TB drugs. However, mycobactericidal potential of nanoparticles towards drug-resistant TB is not confirmed yet. This work explores the bactericidal potential of Zinc Oxide Nanoparticles (ZnONPs, 40 nm) in managing both drug-sensitive and drug-resistant TB in combination with anti-TB drugs. It was found that ZnONPs inhibit generation of active SufB protein via splicing inhibition, an essential event for *Mycobacterium tuberculosis* (*Mtb*) survival. While TEM and UV-visible spectroscopy identified NPs~protein interaction, SEM visualised extensive membrane damage in H37Rv and multidrug-resistant (MDR) *Mtb* cells. Alamar blue assay and spread plate method detected minimum inhibitory concentration and minimum bactericidal concentration of ZnONPs towards H37Rv strain and MDR *Mtb* isolates. *In vitro* studies identified a combination with ZnONPs that reduced effective doses for anti-TB drugs towards H37Rv and MDR *Mtb* isolates.

A correlation to splicing inhibition was made by performing Alamar blue assay in SufB intein-less microbe, *Mycobacterium smegmatis*. A similar drug combination, attenuated the mycobacterial load, inflammation in the spleen & lungs, and protected against *Mtb* induced splenomegaly in infected mice. Thus, ZnONPs can be used as potent additive in anti-TB regimen to manage drug-susceptible and drug-resistant TB, addressing challenges such as prolonged therapy, drug toxicity and poor patient compliance.

Keywords: *Mycobacterium tuberculosis* H37Rv**;** SufB Intein; splicing regulation; ZnONPs; NPs/anti-TB drug combination; Drug-resistant TB

Running title: ZnONPs exhibit bactericidal activity towards MDR *Mtb*

Number of Figures: 8

1. Introduction

Tuberculosis (TB) is one of the leading causes of death worldwide, ranking among the top ten deadliest diseases globally, and is the single most lethal infectious agent, surpassing even HIV/AIDS [1,2]. However, efforts to combat TB are often impeded by several challenges, including absence of an effective vaccine, the complexities of treatment regimens, and the rapid emergence of drug-resistant *Mycobacterium tuberculosis* (*Mtb*) strains [3,4]. Moreover, prolonged therapy can lead to the phenomenon of cross-resistance, where bacteria become resistant to multiple drugs by exploiting shared mechanisms of action [5]. The standard treatment for drug-susceptible and drug-resistant TB spans approximately 6 months and over 18 months, respectively. The intricacy of these regimens, along with drug-induced side effects, often leads to poor patient compliance, worsening the current situation due to the emergence of new drug-resistant strains [6]. Hence, there is an urgency to develop next-generation strategies to mitigate the limitations and enhance the accessibility of TB management .

One promising approach to control TB could be targeting the intein splicing, which is a critical intracellular process that enables *Mycobacterium tuberculosis* (*Mtb*) survival and persistence by generating essential proteins [7,8]. Inteins are intervening polypeptides co-translated within the host precursor proteins and self-excised through protein splicing to generate active protein [9]. Given, that several human pathogens harbour inteins within vital proteins, and intein splicing is critical for their survival, the regulation of splicing can function as a promising target for developing anti-microbial drugs especially towards drug-resistant organisms. *Mtb* SufB, which is an Fe-S cluster assembly protein represents a notable example among mycobacterial proteins, for its significance in disease pathogenesis [10,11]. The SUF system as a whole is required for metalloprotein biogenesis and plays an important role in mycobacterial survival during iron limitation including oxidative and nitrosative stresses within infected macrophages [12,13].

In recent years, the synergistic integration of nanotechnology and medicine has emerged as a popular and diverse approach, particularly for the development of anti-microbial compounds. The convergence of these disciplines has demonstrated significant potential in addressing various challenges associated with bacterial infections [14–16]. Further, the interaction between nanoparticles and proteins holds significant importance in various areas of contemporary biomedical research, particularly in the fields of nanomedicine and nano diagnostics [17–21]. When nanoparticles interact with proteins, they form a protein corona, which alters the biological activity of the bound protein. This phenomenon has profound implications for understanding the behaviour of nanoparticles within biological environments and their potential applications in drug delivery, diagnostics, and therapeutics [22–29].

Thus, nanotechnology is gaining popularity as the cornerstone of modern research and therapeutics. This frequently involves metal based NPs like ZnONPs that offer varied uses in emerging applications such as antimicrobial, anti-inflammatory, anti-tumour, in wound

77 healing, and in enhanced drug delivery systems [30–34]. ZnONPs are reportedly more bio-reactive
78 than the conventional antimicrobials, due to their smaller size and higher surface area to
79 volume ratio [35]. Further, ZnONPs are considered as GRAS (generally recognized as safe)
80 substance [36,37]. Owing to their potent antibacterial and antifungal nature, ZnONPs are widely
81 used in medicine for dermatological applications and in cosmetics [38]. ZnONPs are also
82 preferred as efficient drug delivery vehicles for various diseases including cancer, because of
83 their safety, stability, and low cost [35,39].
84 Previous research have shown the bacteriostatic effects of ZnONPs towards both drug-sensitive
85 and extensively drug-resistant (XDR) *Mtb* strains at concentrations equal to or higher than 1
86 µg/ mL [40]. The same study has also determined 4 µg/mL as the inhibitory concentration of
87 ZnONPs against the multidrug-resistant (MDR) strain of *Mtb*. Another work has reported the
88 bactericidal role of ZnONPs - Se against *Mtb* BCG and H37Rv strains [41]. The antimicrobial
89 mechanisms for ZnONPs effects are mostly attributed to a cumulative effect of cell membrane
90 disruption, ROS production, release of toxic Zn^{+2} ions, and toxicity induced by their
91 photocatalytic action [42]. Although ZnONPs are known to exhibit potent antimicrobial and
92 fungicidal activity towards different microbes [43], their bactericidal potential on drug-resistant
93 *Mtb* strains are not shown till date. In a different context, inhibitory effects of divalent metal
94 ions such as Zn^{+2}, and Cu^{+2} on the splicing of various intein containing precursor proteins were
95 explored extensively, but studies showing intein splicing attenuation in presence of metal-
96 based NPs is missing till date [8,44–49].
97 Current study addresses the following questions: 1) Whether ZnONPs can regulate
98 *Mycobacterium tuberculosis (Mtb)* SufB intein splicing and N-terminal cleavage reactions? 2)
99 Since intein splicing generates a functional SufB protein that is critical for mycobacterial
100 survival, whether ZnONPs mediated regulation of SufB splicing can affect the viability of
101 whole cell *Mtb?* 3) Importantly, if, the viability of both drug-sensitive and drug-resistant strains

102 of *Mtb* are influenced by ZnONPs? Next, 4) what is the minimum effective concentration of
103 ZnONPs for the observed effect? 5) Whether ZnONPs combination can reduce the required
104 dosage of existing anti-TB drugs to control both drug-sensitive and drug-resistant *Mtb*
105 infection? 6) Whether ZnONPs exhibit a bacteriostatic or bactericidal effect towards drug-
106 sensitive and drug-resistant *Mtb* strains*?* 7) Can ZnONPs protect against the effects of *Mtb*
107 infection in an animal model?
108 In this work, ZnONPs (40 nm) activity on the splicing and N-terminal cleavage reactions of
109 the *Mycobacterium tuberculosis* (*Mtb*) SufB precursor protein was examined. Initial
110 cytotoxicity evaluation via MTT assay indicated that ZnONPs are biocompatible towards
111 HEK293T cells (human embryonic kidney cell lines), up to a concentration of 50 µg/ml,
112 consequently rest of the experiments were performed within this limit. UV-Vis spectroscopy
113 confirmed ZnONPs ~ SufB interaction, further supported by Transmission Electron
114 Microscopy (TEM), which identified protein "corona" formation around the ZnONPs. Next,
115 ZnONPs over varied concentration range (0.5 µg/ml-50 µg/ml) significantly inhibited the
116 splicing and N-terminal cleavage reactions of *Mtb* SufB precursor protein as shown by *in vitro*
117 protein refolding assay. SDS-PAGE and Western blot analyses visualized and confirmed the
118 splicing and cleavage products. Further, Alamar blue assay and spread plate method detected
119 anti-mycobacterial activity of ZnONPs with a minimum inhibitory concentration (MIC) /
120 minimum bactericidal concentration (MBC) of 5 µg/ml/17 µg/ml and 14 µg/ml/23 µg/ml
121 towards H37Rv strain (drug-sensitive) and multidrug-resistant (MDR) *Mtb* isolates
122 respectively. In a comparative study, we also observed a reduction in the effective dose of
123 anti- TB drugs INH/RIF and LFX/MXF in combination with ZnONPs that could efficiently
124 kill H37Rv strain and multidrug-resistant (MDR) *Mtb* isolates respectively. The observed
125 activity was correlated to splicing inhibition by performing Alamar blue assay in SufB intein-
126 less microbe *Mycobacterium smegmatis*. Scanning Electron Microscopy (SEM) demonstrated

127 mycobactericidal activity of ZnONPs towards both drug-sensitive and drug-resistant *Mtb*
128 (H37Rv) strains. Finally, infected mice model study revealed that ZnONPs in combination with
129 anti-TB drugs can effectively reduce mycobacterial load in the lungs and spleen. The observed
130 effects were noticed when ZnONPs was administered as a solo therapy or in combination with
131 a reduced dose of RIF compared to previously recommended amount of RIF. Likewise, the
132 same combination of ZnONPs - RIF, not only attenuated the inflammation in lungs and spleen,
133 but also provided resistance to splenomegaly in the infected mice. Therefore, we suggest the
134 use of ZnONPs as a promising adjunctive therapy along with standard anti-TB drugs to combat
135 both drug-sensitive and multidrug-resistant *Mtb* infections, by inhibiting the splicing of an
136 essential protein, *Mtb* SufB. This approach may not only mitigate the toxicity associated with
137 conventional and contemporary anti-TB regimens but also potentially reduce the duration of
138 therapy, thereby enhancing patient compliance.

139 **2. Materials and Methods**

140 *2.1 ZnO nanoparticles*

141 ZnONPs (≥ 40 nm) were procured from Sigma Aldrich (Product #721077).

142 *2.2 MTT Assay* [50–52]

143 The cytotoxic effects of ZnONPs were evaluated using the MTT (3-[4,5-dimethylthiazol-2-yl]-
144 2,5-diphenyltetrazolium bromide) assay over a period of 72h. HEK239T cells (10^4 cells/well)
145 [Product # HEK239T (Human embryonic kidney cell line, ATCC (CRL-3216)] were seeded in
146 Dulbecco's Modified Eagle Medium (DMEM, Gibco, Invitrogen-2562497) in a 96-well plate
147 (200 µl per well) and allowed to adhere for 24 hours at 37°C in 5% CO_2 incubator.
148 Subsequently, varying concentrations of ZnONPs (5 µg/ml, 14 µg/ml, 17 µg/ml, 23 µg/ml
149 µg/ml, 26 µg/ml, 50 µg/ml, 100 µg/ml, 150 µg/ml) were added, followed by incubation at
150 37°C in 5% CO_2 incubator for 72 hours. HEK239T cells (10^4 cells/well) incubated in absence

151 of nanoparticles was considered as the control for 100% viable cell growth. DMEM culture
152 medium alone was used as blank control. 20 µl of MTT (EZcount™ MTT cell assay kit,
153 Himedia-CCK003) solution (5 mg ml^{-1} in incomplete medium) was added to each well and
154 incubated for 3h to facilitate formation of purple formazan crystals under standard culture
155 conditions. Next, MTT solution was discarded, and the crystals were solubilized by gently
156 stirring on orbital shaker for 30 minutes. After solubilization, the absorbance (570 nm) of each
157 well was measured by using the ELISA plate reader (Bio Teck Epoch Microplate
158 Spectrophotometer). The percentage of cell viability was calculated using the following
159 formula.

160 $$\%\ of\ Cell\ viability = \frac{optical\ density\ (OD570) test\ sample - optical\ density\ (OD570) blank\ control}{OD570\ growth\ control - OD570\ blank\ control} \times 100$$

161 *2.3 UV Visible spectroscopy* [53–55]

162 Purified *Mtb* SufB precursor protein was refolded in presence of different concentrations of
163 ZnONPs (0.5 µg/ml, 26 µg/ml, and 50 µg/ml) as explained in section 2.7 for *in vitro* refolding
164 assay. Then, the treated samples were analyzed via UV-Visible spectroscopy (UV-1800
165 Shimadzu) over the visible region of the spectrum (200-800 nm). To account for potential
166 buffer-nanoparticle interactions, control samples included refolding buffer (20 mM sodium
167 phosphate, 0.5 M NaCl, 0.5 M arginine, and 8 M urea) alone and the buffer with 50 µg/ml of
168 nanoparticles incubated under the same conditions. The nanoparticle-treated buffer served as a
169 blank for baseline correction. The absorbance results were analyzed by plotting absorbance
170 versus wavelength using OriginPro 8.5 (Version 8.5, OriginLab Corporation, Northampton,
171 MA, U.S.A.).

172 *2.4 Quantification of NPs-bound proteins via Bradford assay* [56–58]

173 The quantification of adsorbed protein was conducted using the Bradford assay. *Mtb* SufB
174 precursor protein was renatured *in vitro* both in presence and absence various concentrations

175 of ZnONPs (0.5 µg/ml, 26 µg/ml, and 50 µg/ml) for 4 hours, as mentioned in section 2.7. Next,
176 the protein-NPs mixture was centrifuged at 13,000 rpm for 30 minutes, at 4°C, to separate the
177 protein-bound nanoparticles. Then, the pellet containing the protein ~ NPs was resuspended in
178 100 µl of 1X PBS and analysed using Bradford reagent to quantify the amount of adsorbed
179 proteins. Control samples included nanoparticles in 1XPBS and test proteins resuspended in
180 1XPBS.

181 *2.5 TEM Analysis* [59,60]

182 *Mtb* SufB precursor protein-ZnONPs interaction was analysed by Transmission Electron
183 Microscope (Jeol JEM-1400) for visualising protein corona formation. *Mtb* SufB precursor
184 protein was overexpressed, purified and refolded with 50 µg/ml of ZnONPs as mentioned in
185 section 2.7. The protein-ZnONPs complex was collected via centrifugation (13,000 rpm for 30
186 minutes) at 4^0C, washed twice with phosphate buffer saline (1X PBS) and the supernatant
187 was discarded. Then the pellet (protein-ZnONPs complex) was resuspended and fixed with 100
188 µl of 2.5% glutaraldehyde in 1X PBS, for 1 hr. Finally, 5 µl of solution (ZnONP-complex)
189 was placed onto the carbon-coated copper grid and imaged under TEM with an acceleration
190 voltage of 120 Kv.

191 *2.6 Purification of overexpressed proteins*

192 The details of the plasmids used in this study are provided elsewhere [7]. The *Mtb* SufB wild
193 type precursor, and *Mtb* SufB splicing inactive double mutant (C1A/N359A) (splicing negative
194 control), all carrying an N-terminal 6X His tag, were overexpressed in BL21 (DE3) *E. coli* cells
195 via IPTG (500 µM, sigma 367-93-1) induction. The cells were resuspended in lysis buffer
196 (20mM sodium phosphate, 0.5M NaCl, pH 7.4) and lysed using a tip sonicator (Sonics vibra
197 cell VCX-130) [61]. The cell lysate was centrifuged at 16,500xg for 20 minutes at 4°C and the
198 supernatant was discarded. The collected IB materials were washed thrice via centrifugation in

199 lysis buffer, solubilized in 8 M urea (Merck, 1084870500) buffer (lysis buffer, 8M urea, 10
200 mM imidazole (MP–biochemicals-288-32-4), and centrifuged at 16,500xg for 20 minutes at
201 4°C to collect the supernatant. The solubilized proteins were purified using a Ni-NTA affinity
202 column (Ni-NTA His trap, HP GE healthcare life sciences- 17524802) [62–66]. Before sample
203 application, the columns were equilibrated with binding buffer (20 mM sodium phosphate, 0.5
204 M NaCl, 8 M urea, 10 mM imidazole), and after loading the samples, the columns were washed
205 several times (15 column volumes) with the wash buffer (20 mM sodium phosphate, 0.5M
206 NaCl, 8M urea, 40 mM imidazole). Finally, the test proteins were eluted in elution buffer
207 (20mM sodium phosphate, 0.5M NaCl, 500 mM imidazole, 8 M Urea, pH 7.4) and quantified
208 using Bradford's assay.

209 *2.7 In vitro protein refolding and splicing analysis via SDS gradient PAGE*

210 Denatured test proteins (2.5 µM) in 8M urea buffer were renatured in a refolding buffer
211 containing 20 mM sodium phosphate, 0.5 M NaCl, 0.5 M L-Arginine (A5006 Sigma Aldrich),
212 and 2 mM TCEP-HCl (Sigma-51805-45-9). Protein refolding was performed for 4 hours at
213 25ºC [61–66] in the presence and absence of ZnO nanoparticles (ZnONPs) over a varied
214 concentration range (0.5 µg/ml to 50 µg/ml). For the 0-hour sample, protein sample was
215 collected before initiation of the refolding, followed by immediate addition of the loading dye
216 (0.1% bromophenol blue, 50% glycerol, β-mercaptoethanol, 10% SDS, tris, pH 6.8) and rapid
217 freezing at -20ºC. After 4h of protein renaturation, rest of the samples were collected, loading
218 dye was added, samples were boiled at 95ºC for 5 minutes. Then protein products were resolved
219 through 5~10% gradient SDS-PAGE gel. The protein bands were visualized by staining with
220 Coomassie brilliant blue R-250 (Catalogue no #112553, Sigma-Aldrich), and densitometric
221 analysis was performed using the GelQuant.Net biochemical solutions software. The splicing
222 and cleavage efficiencies were calculated as the percentage ratio of the total splicing product
223 (LE and I) over the total proteins (LE+I+P) and the total N-terminal cleavage product (NE+NC)

224 over the total proteins (NE+NC+P), respectively. 0-hour splicing and cleavage product values
225 were subtracted from respective sample values for baseline corrections. The results were
226 analysed using one-way ANOVA and plotted using GraphPad Prism version 5.01 for
227 Windows, GraphPad Software, San Diego, CA, U.S.A., www.graphpad.com.

228 *2.8 Western blot analysis* [8]

229 For Western blot analysis, an anti-His antibody was utilized to confirm the presence of splicing
230 and N-terminal cleavage products. The test proteins were transferred from the 5-10% SDS-
231 PAGE to the PVDF membrane (Millipore, IPVH 00010) at a voltage of 10V, overnight at 4ºC.
232 Subsequently, the blot was blocked with 5% skim milk and incubated overnight at 4ºC. Then,
233 the membrane was washed once with 1X TBST (Tris-buffered saline with Tween-20) followed
234 by incubation with a primary anti-His antibody (abgenex-32-6116) at 1:5000 dilution
235 overnight at 4ºC. In the next step, the membrane was washed thrice for 5 minutes, with 1X
236 TBST and incubated with a secondary antibody (anti-mouse, abgenex 11-301) at a dilution of
237 1:6000, for 6 hours at 25ºC. To enhance detection of the N-extein band, a higher dilution of the
238 primary antibody (1:2500) and secondary antibody (1:4000) were used. Finally, the blots were
239 washed with 1X TBST and developed using Enhanced Chemiluminescence Substrate (ECL)
240 (abcam, ab65628) to visualize the protein bands and images were captured using in-house
241 ImageQuant™ LAS 500 facility (GE Healthcare).

242 *2.9 Anti-mycobacterial study*

243 *2.9.1 Preparation of Mtb cells* [67]

244 Different mycobacterial cells [Drug sensitive H37Rv (ATCC-27294), H37Ra (ATCC-25177),
245 *M.sm* (ATCC-19420) and clinically isolated MDR *Mtb* isolates obtained from National
246 Reference Laboratory (NRL), ICMR-Regional Medical Research Centre (RMRC-ICMR),
247 Bhubaneswar, India] were grown in Middlebrook 7H9 broth (Merck-M0178) supplemented

248 with Middlebrook oleic acid, albumin, dextrose, and catalase (OADC) (Himedia-FD018). CFU
249 calculations were made by matching the turbidity of inoculum with McFarland standard
250 (Himedia- R092) against a black background. 10^6 CFU of mycobacterial cells were used for
251 subsequent experiments.

252 *2.9.2 Alamar blue assay* [68–70]

253 10^6 CFU of mycobacterial cells were incubated with different concentrations of ZnONPs (0.5
254 ug/ml to 50 ug/ml) in 96-well microtiter plates. For a comparative study, cells were also
255 incubated with anti- TB drugs Isoniazid (INH), Rifampicin (RIF), Moxifloxacin (MXF), and
256 Levofloxacin (LFX) to evaluate their activity towards H37Rv strain and multidrug-resistant
257 (MDR) *Mtb* isolates. The plates were sealed and incubated at 37ºC for 14 days. Later, 10%
258 (v/v) solution of Alamar Blue reagent (SRL-42650) was added to each well and the plates were
259 incubated at 37ºC for 24 hours. The anti-mycobacterial efficacy of each compound was
260 evaluated based on the observed colour change. Live cells were identified by transition of
261 colour from blue to pink whereas dead cells remained blue. The minimum inhibitory
262 concentration (MIC) for ZnONPs and anti-TB drugs were determined as the lowest
263 concentration at which cell viability was inhibited partially, resulting in a purple colour.

264 *2.9.3 Spread plate method to determine Minimum Bactericidal Concentration (MBC)* [71]

265 Mycobacterial cells at 10^6 CFU were incubated with different concentrations of ZnONPs (0.5
266 μg/ml to 50 μg/ml) for 14 days in 96 well microtiter plates. Then, sample (1:1000 dilution)
267 from each well was evenly spread onto respective 7H10 agar (Himedia- M199) plate using a
268 sterile spreader. The plates were incubated at 37ºC for 21days to grow mycobacterial colonies.
269 Subsequently, colonies were counted by colony counting method and MBC was determined as
270 the lowest concentration of the test compounds at which no colony growth was visualised on
271 the respective agar plates. Controls plates included mycobacterial cells without NPs treatment.
272

273 *2.9.4 Scanning Electron Microscopic (SEM) analysis* [72]

274 10^6 CFU of mycobacterial cells were incubated with different concentrations (0.5 µg/ml,17
275 ug/ml, 26 µg/ml, and 50 µg/ml) of ZnONPs in 7H9 broth medium for 7 days. Then, cells were
276 harvested, fixed with 2.5% glutaraldehyde, and dehydrated with a series of ethanol treatment
277 (30%, 60%, 70%, 80%, and 90%). Finally, cells were treated with 100% ethanol for 30 min.
278 Then gold-palladium particles were sputtered over the mycobacterial cells by an automated
279 sputtering machine and visualized via SEM (Hitachi, S-3400N), CIF, OUAT, Bhubaneswar.

280 *2.9.5 Animal experiments* [68]

281 Female BALB/c mice, aged 6 to 8 weeks and weighing each 25 ± 2 g, were used for the study.
282 Mice were randomly divided into three groups, each consisting of 6 to 8 mice. The animals
283 were injected intravenously with 5 x 10^6 colony-forming units (CFU) of *Mycobacterium*
284 *tuberculosis* (strain H37Ra) over a period of 4 days. Subsequently, ZnONPs were orally
285 administered to the infected mice at different concentrations (26 and 50 µg/ml) for 7 days post-
286 infection. Rifampicin alone, given orally at a dose of 15 mg/kg to the infected mice was used
287 as a positive control, while mice who were given oral 1X PBS served as the negative control.
288 After 18 days of infection, the mice were euthanized under 5% inhaled isoflurane anaesthesia
289 (Sigma-792632), followed by cervical dislocation. Then, their lungs and spleen were isolated
290 and processed for histopathological examination and estimation of mycobacterial load via CFU
291 analysis. A portion of the lung was fixed in 4% paraformaldehyde for 48 hours and then
292 embedded in paraffin to prepare sections for haematoxylin and eosin staining. Next, lung and
293 spleen homogenates in 1X PBS were plated onto Middlebrook 7H11 agar, supplemented with
294 OADC (Himedia-FD018) and BBL MGIT PANTA antibiotics (Catalogue #245114, BD,
295 United States), to quantify the bacterial burden. Culture plates were incubated for 3 to 4 weeks
296 at 37°C, followed by calculation of CFU by colony counting methods.

297

298

299 *2.10 Statistical analysis*

300 For each method, numerical data from three to six independent sets of experiments were
301 analysed using GraphPad Prism 6.0 (La Jolla, CA, United States) and are presented as mean ±
302 1 standard deviation or standard error of the mean. Statistical significance between different
303 groups was assessed using one-way ANOVA, with significance denoted by $p < 0.05$. Specific
304 p-values of <0.05, <0.01, <0.001, and <0.0001 were indicated as *, **, ***, and ****,
305 respectively.

306 **3. Results and discussions**

307 *3.1 ZnONPs interact with Mtb SufB precursor protein*

308 Previous studies have reported interaction of nanoparticles with biological molecules such as
309 proteins and DNA [73]. Before examining the role of ZnONPs on the splicing activity, we
310 evaluated possible interaction between ZnONPs and *Mtb* SufB precursor protein. Through a
311 combination of analytical techniques such as UV-visible spectroscopy, Bradford analysis, and
312 transmission electron microscopy (TEM), we have evaluated ZnONPs~protein binding activity
313 (Figure 1).

314 Initially, cytotoxicity of the ZnONPs was assessed via MTT assay using human embryonic
315 kidney cell line, HEK239T cells, since potentially harmful NPs are mostly excreted by kidney
316 through urine [74–76]. It was demonstrated that up to a concentration of 50 µg/ml, ZnONPs
317 exhibited no cytotoxicity against HEK239T cells (Figure S1, Supplementary Information).
318 This is further supported by a prior research which has shown similar results [77]. Consequently,
319 we decided to explore SufB interaction with various ZnONPs concentrations up to this limit
320 (0.5, 26, and 50 µg/ml). UV–Visible spectra for both the *Mtb* SufB precursor protein and
321 ZnONPs-SufB complexes were recorded by scanning over the visible range (200 to 800 nm),
322 as depicted in Figure 1A. Buffer alone and buffer along with nanoparticles (50 µg/ml) were

323 used for baseline correction and as the reference blank respectively. An observable broadening
324 and blue shift were differentiated in the absorbance spectra of the *Mtb* SufB protein following
325 interaction with increasing concentrations of ZnONPs, when compared to the spectra of protein
326 solubilised in buffer alone. This observation suggests the binding of ZnONPs with the *Mtb*
327 SufB precursor protein over test concentration range.
328 To further validate such interaction, we utilized Bradford assay, where *Mtb* SufB precursor
329 protein was refolded along with varying concentrations of ZnONPs (0.5, 26, and 50 µg/ml),
330 causing adsorption of proteins onto the NPs surface. After isolating ZnONPs-protein
331 complexes, quantification of bound proteins was done using Bradford assay. As illustrated in
332 Figure 1B, an increase in nanoparticle concentration correlated with a proportional increase in
333 the bound proteins. This result further supported the interaction between ZnONPs and *Mtb*
334 SufB protein.

335 The formation of a protein corona on NPs surfaces was investigated through TEM analysis, as
336 shown in Fig 1C. While standalone ZnONPs exhibited discrete distribution [1C(i)], NPs (50
337 µg/ml)-treated protein sample displayed a distinct feature. A thin, transparent layer encasing
338 the NPs was evident in the treated sample (yellow arrows) as seen in the Figures 1C(ii and iii).
339 This is indicative of the protein corona formed on the surface of the ZnONPs upon interaction
340 with the *Mtb* SufB protein [78].

341 The comprehensive assessment involving UV-visible spectroscopy, Bradford analysis, and
342 TEM, successfully indicated the binding activity and protein corona formation following
343 ZnONPs interaction with *Mtb* SufB.

344

345

346

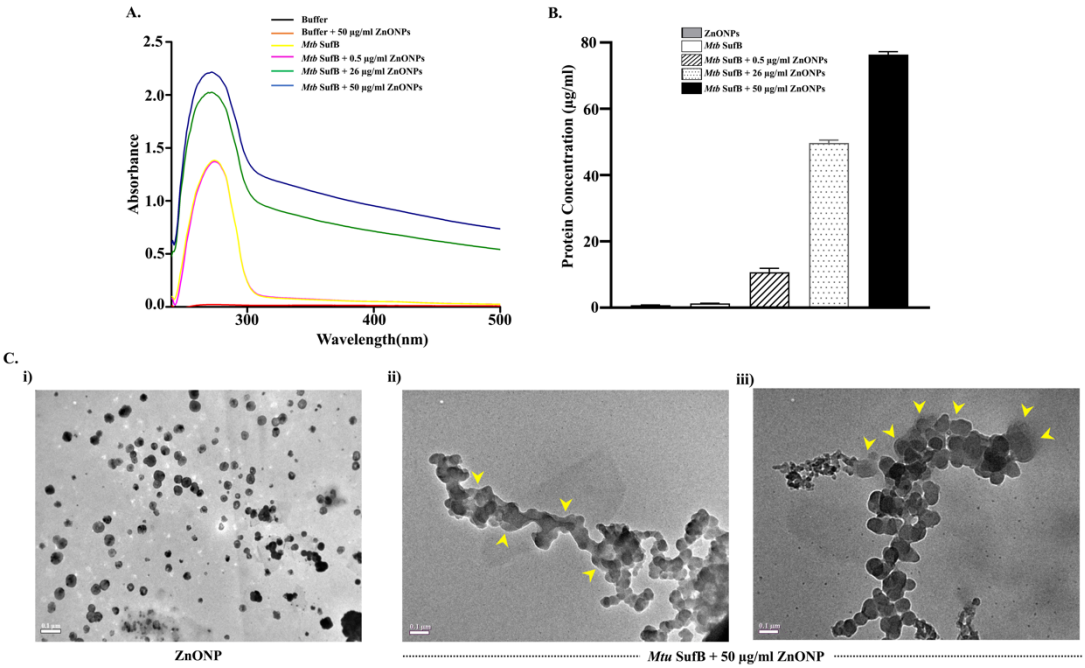

Figure 1. Evaluation of ZnONPs interaction with *Mtb* SufB. A) UV–Visible spectroscopy: *Mtb* SufB precursor protein was treated with ZnONPs (0.5 µg/ml, 26 µg/ml, 50 µg/ml) and sample absorbance was measured by scanning over 200–500 nm wavelength. **B)** Bradford Assay: Denatured test proteins were renatured *in vitro* in the presence of varied ZnONPs concentration for a period of 4 hrs at 25^0C. Then test samples were processed and the concentration of adsorbed protein was determined using Bradford reagent. **C)** TEM Analysis: Images showing. (i) discrete ZnONP, and (ii) & (iii) protein corona formation on the surface of ZnONPs aggregates after interaction with *Mtb* SufB.

3.2 *ZnONPs inhibit generation of functional SufB protein*

The SUF system provides an unique pathway for [Fe-S] cluster biosynthesis and *Mtb* survival during intracellular stress like iron deprivation [79]. In such environments, the functionality of the SUF complex relies exclusively on the splicing of *Mtb* SufB precursor to generate active SufB protein [13]. Hence, splicing regulation under such physiological stress can lead to potential anti-TB drug development strategies by influencing mycobacterial cell viability. Although metals are known inhibitors of intein splicing [44,47,48], NPs mediated splicing inhibition has not been reported yet. Further, higher reactivity of nanoparticles in a biological system has

376 prompted us to evaluate ZnONPs and *Mtb* SufB interactions with possible effects on SufB
377 precursor splicing.

378 *In vitro* splicing assay was conducted both in the presence and absence of ZnONPs, as detailed
379 in the methods section. Since, MTT assay demonstrated that HEK239T cells (human
380 embryonic kidney cell lines) were tolerant to ZnONPs up to a concentration of 50 µg/ml (Figure
381 S1, Supplementary Information), splicing efficiency was evaluated using NPs concentrations
382 up to this limit. Figure 2A illustrates different structural domains of *Mtb* SufB precursor
383 protein; N-extein (29.9 kDa), Intein (40.2 kDa), and C-extein (25.8 kDa). The details of *Mtb*
384 SufB splicing and N- terminal cleavage reactions are published elsewhere [7]. SufB precursor
385 undergoes splicing reactions to generate ligated exteins (LE), and intein (I), whereas N-
386 terminal cleavage reactions yield N-terminal cleavage product (NC, 65.2 kDa), and N-extein
387 (NE) (Figure 2A). Figures 2B(i) and 2B(ii) depict the concentration-dependent inhibition of
388 these reactions by ZnONPs, providing crucial insights into their biological role.

389 The samples were analyzed through gradient SDS-PAGE, and the bands were quantified using
390 the GelQuant.NET software. Our findings indicated a substantial inhibition of *Mtb* SufB
391 precursor splicing ($p<0.0001$) over all the test concentration range, with discernible effects
392 commencing at a ZnONPs concentration of 0.5 µg/ml. Remarkably, a complete inhibition of
393 splicing was observed at a concentration of 47 µg/ml [Figures 2B(ii) and C(i)]. These findings
394 suggest that ZnONPs exert a dose-dependent inhibition of splicing in *Mtb* SufB precursor
395 protein which could lead to critical consequences such as loss of functionality of this protein
396 in a cellular environment.

397 Similarly, the N-terminal cleavage reaction of *Mtb* SufB precursor was notably inhibited
398 ($p<0.0001$) in the presence of ZnONPs. A reduction in the cleavage activity was observed at
399 the minimal tested concentration of 0.5 µg/ml, culminating in a complete inhibition at a

400 concentration of 26 µg/ml [Figures 2B(i) and C(ii)]. Thus, ZnONPs exert a potent inhibitory
401 effect on the *Mtb* SufB splicing and N-terminal cleavage reactions, underscoring their potential
402 interference with SufB-associated cellular processes. These findings also highlight the
403 significant biological implications of ZnONPs on *Mtb* survival within host cells. To
404 substantiate these findings, we performed western blot analysis to validate identity of protein
405 products (Figure S2, Supplementary Information), which further confirmed the inhibitory role
406 of ZnONPs on the splicing and N-terminal cleavage reactions of SufB.

407 Current research presents evidence that ZnONPs interact with the *Mtb* SufB precursor protein,
408 leading to a concentration-dependent inhibition of both splicing and N-terminal cleavage
409 reactions. These findings also emphasize on the notable impact ZnONPs could have on the
410 essential cellular processes linked to *Mtb* SufB protein, and their potential implications in
411 biological systems. Specifically, it calls for further exploration into the influence of ZnONPs
412 on SufB splicing, correlating this process to the growth and viability of *Mtb.*

413

414

415

416

417

418

419

420

421

422

423

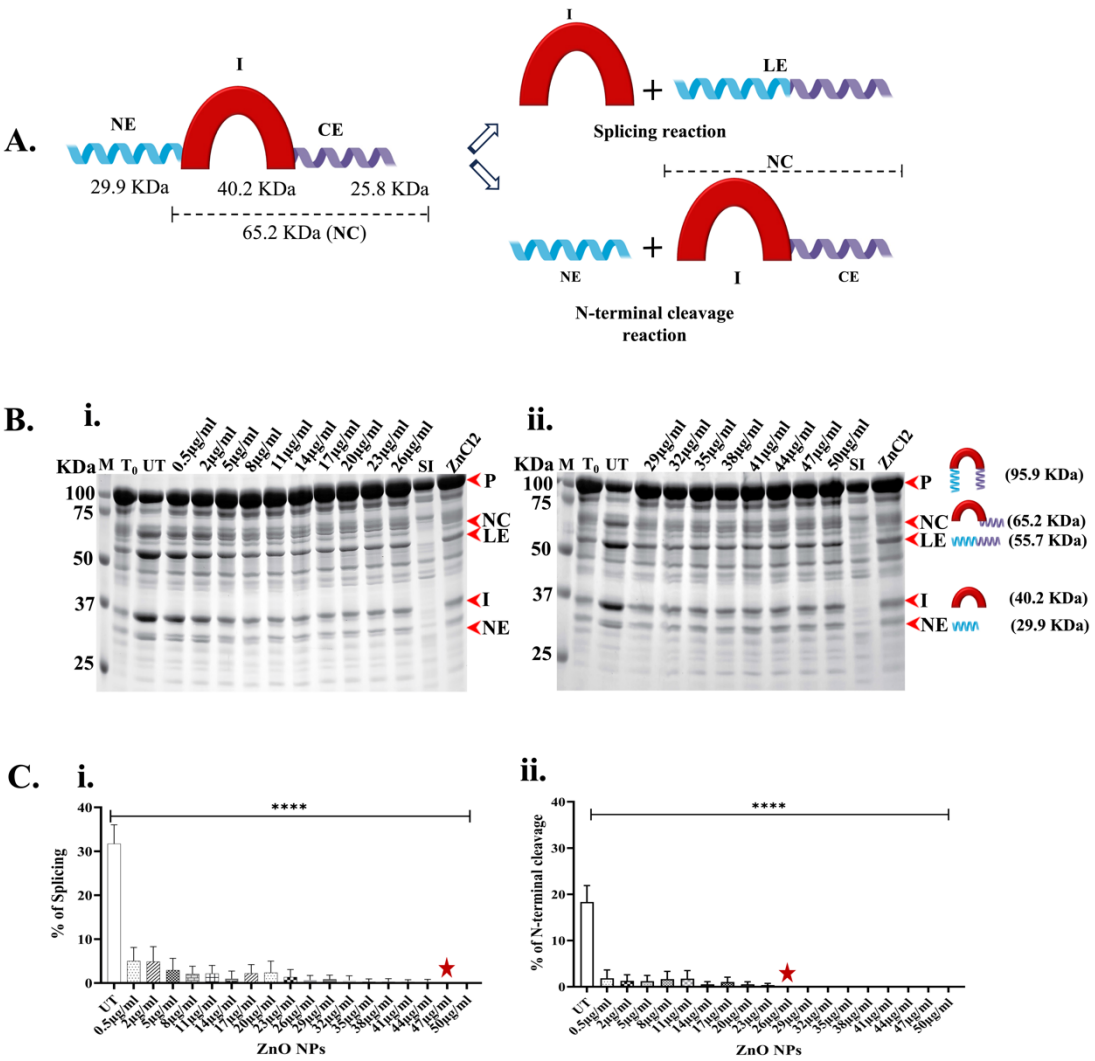

Figure 2. Effect of ZnONPs on *Mtb* SufB precursor splicing and N-terminal cleavage reactions. (A) Schematic diagram representing different structural domains of *Mtb* SufB precursor protein and splicing & N-terminal cleavage reactions of the precursor protein generating different protein products. **(B)** Products from *in vitro* protein refolding experiment were resolved through 5–10% gradient SDS-PAGE. (T_0): splicing and cleavage reactions at 0 h, (UT): untreated protein sample; and Lanes 4- 13 show protein products induced by varied concentrations ZnONPs: (i) (0.5 µg/ml -26 µg/ml) (ii) (29 µg/ml to 50 µg/ml), Lane 14 (SI): Splicing inactive SufB double mutant (Cys1Ala/Asn359Ala) is used as a negative control for splicing, Lane 15: $ZnCl_2$ (2 mM) was used as a positive control, since it is a known inhibitor of *Mtb* SufB splicing reactions [8]. **(C)** Bar graphs showing the quantitative values of splicing (i), and N-terminal cleavage (ii) reaction inhibition as shown in Fig. 2(B). These were plotted after densitometric analyses using GelQuant.Net biochemical solutions. 0h splicing, and cleavage values were subtracted from each sample as baseline correction. Red stars denote complete inhibition of SufB splicing and N-terminal cleavage reactions by ZnONPs at concentration 47 µg/ml and 26 µg/ml respectively. Error bars represent (±1) SEM from (n=3) three independent sets of experiments

453 (p<0.0001). P: precursor, NC: N-terminal cleavage product, LE-: ligated extein, I- intein, and NE: N-
454 extein.
455
456 *3.3 ZnONPs inhibit the growth and viability of Mycobacterial cells*
457 Since ZnONPs were shown to interact with the SufB precursor protein, and caused inhibition
458 of protein splicing, it was imperative that this may retard the growth and viability of *Mtb* by
459 blocking the generation of an essential protein SufB. Both H37Rv cells and MDR *Mtb* isolates,
460 were cultured in a nutrient medium along with various concentrations (0.5 µg/ml~50 µg/ml) of
461 ZnONPs, as discussed in the methods section. The test concentration range for the ZnONPs
462 were chosen based on their activity range as outlined in Figures 2B and 2C. Further, up to a
463 concentration of 50 µg/ml, ZnONPs exhibited no cytotoxicity against HEK239T cells (Figure
464 S1, Supplementary Information). Besides, ZnONPs at a concentration of ≥50 µg/ml was also
465 found to be toxic for human cells, elucidated by earlier research [80].
466 We performed Alamar blue assay, a well-established metric for cell viability, which yielded
467 data on the inhibitory roles of ZnONPs on the growth and survival of H37Rv and MDR *Mtb*
468 cells. The Alamar blue dye, initially blue, undergoes reduction in viable cells, resulting in a
469 colour change to pink, whereas persistence of the blue colour indicates lack of viable cells [81].
470 ZnONPs at 0.5 µg/ml and 2 µg/ml did not have any effect H37Rv cells. 5 µg/ml was identified
471 as the minimum inhibitory concentration (MIC) for ZnONPs at which H37Rv cells turned
472 purple due to partial loss of cell viability (Figure 3A). A complete loss of cell viability, and
473 retention of blue colour was noted at a concentration of 17 µg/ml of ZnONPs.
474
475
476
477
478

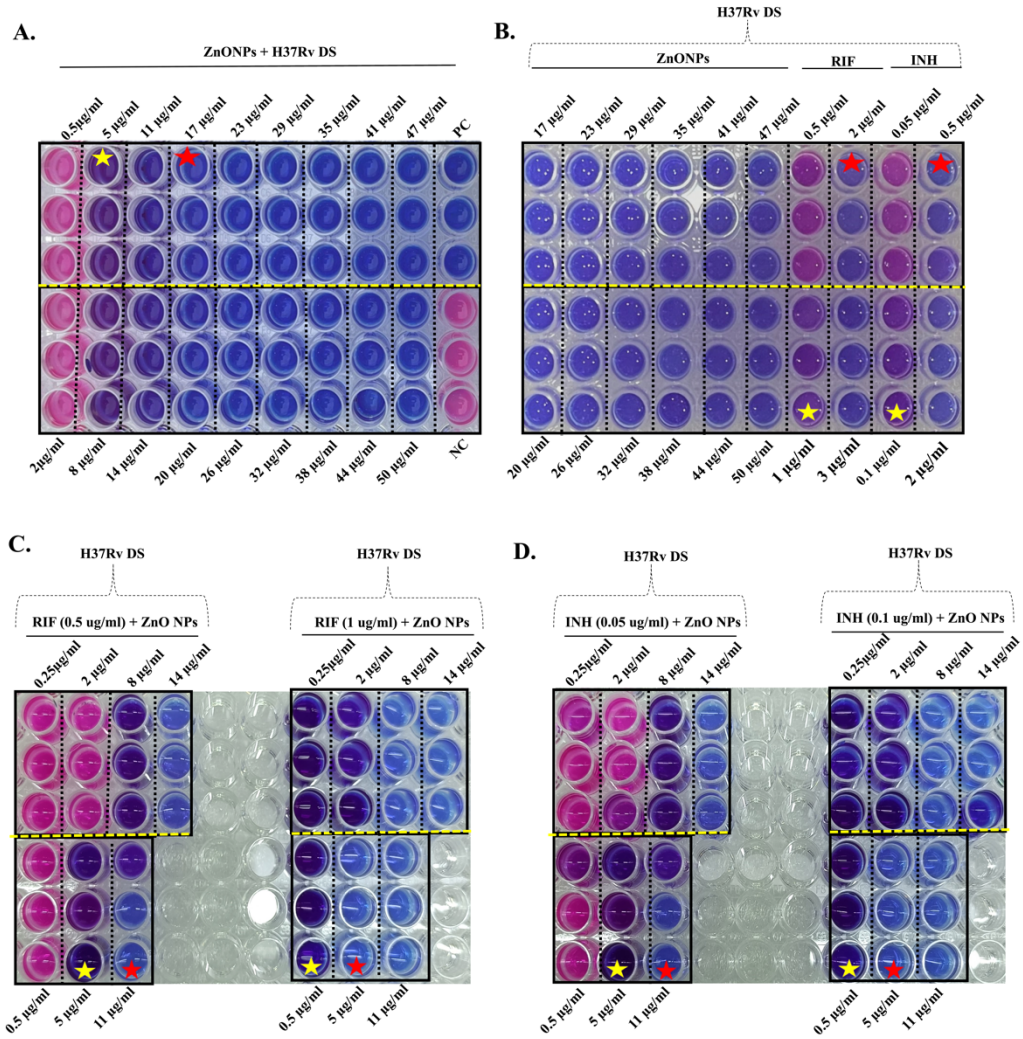

Figure 3. Alamar blue assay to determine the minimum inhibitory concentrations (MIC) of ZnONPs towards H37Rv *Mtb* cells. (A) Mycobacterial cells were incubated in a 96 well plate, in presence of varied concentrations (0.5 to 50 µg/ml) of NPs for 14 days, followed by addition of Alamar Blue reagent. Further incubation at 37ºC for 24 hours, led to colour change in the wells. MIC of ZnONPs was identified as 5 µg/ml where transition of blue to purple colour occurred suggesting partial loss of cell viability among the cells. Persistence of blue colour correlating to complete loss of viable cell population was seen at 17 µg/ml of ZnONPs. Pink cells refer to healthy viable cells resisting inhibitory effect of ZnONPs. **(B)** Comparison of the activity of first line anti-TB drugs; INH & RIF and varied concentration of ZnONPs. All the cells were rendered non-viable (blue) at a concentration of 17 µg/ml for the NPs, 2 µg/ml for RIF, 0.5 µg/ml for INH, and at respective higher concentrations. The MIC for RIF & INH as shown in this study coincided with the known values of 1 and 0.1 µg/ml respectively [82]. Synergistic activity of ZnONPs and anti-TB drugs; **(C)** RIF & **(D)** INH. 10^6 CFU of

508 bacterial cells were grown in presence of varied concentrations of ZnONPs and Drugs. A combination
509 of RIF (0.5 μg/ml)+ ZnONPs (1 μg/ml) & RIF (1 μg/ml)+ ZnONPs (5 μg/ml) successfully yielded
510 non-viable cells (blue). Likewise, INH (0.05μg/ml) + ZnONPs (11 μg/ml) & INH (0.1 μg/ml) +
511 ZnONPs (5 μg/ml) combinations resulted in non-proliferating cells (blue). Red stars- complete loss of
512 viability & Yellow stars- partial loss of viable cells (purple) at a lower concentration of NPs. DS: Drug
513 sensitive H37Rv *Mtb*, RIF: Rifampicin, INH: Isoniazid.
514

515 Next, a comparative study was conducted to assess the efficacy of ZnONPs in tandem with
516 first-line anti-TB drugs such as Rifampicin (RIF) and Isoniazid (INH) for which the Minimum
517 Inhibitory Concentrations (MICs) and Minimum bactericidal Concentrations (MBC) are well-
518 documented [82,83]. RIF and INH, at known MICs of 1 μg/ml and 0.1 μg/ml respectively, resulted
519 in partial loss of mycobacterial cell viability (purple colour) in the respective wells. There
520 was a complete loss of viable cell population (blue colour) at 2 μg/ml of RIF, and 0.5 μg/ml of
521 INH, comparable to the activity of ZnONPs at 17 μg/ml (Figure 3B). All the cells were
522 rendered non-viable at concentrations higher than these values.
523 Figures 3C and 3D depict the synergistic activity of ZnONPs and first line anti-TB drugs; RIF
524 & INH. A combination of RIF (0.5 μg/ml) + ZnONPs (11 μg/ml) & RIF (1 μg/ml) + ZnONPs
525 (5 μg/ml) successfully yielded non-viable cells (blue). Likewise, INH (0.05 μg/ml) + ZnONPs
526 (11 μg/ml) & INH (0.1 μg/ml) + ZnONPs (5 μg/ml) combinations resulted in non-proliferating
527 cells (blue). Thus, both RIF and INH at their respective MIC and half reduced MIC values
528 could completely abolish mycobacterial cell viability when added together with ZnONPs.
529 These results emphasize on the diminution in effective concentration for the conventional anti-
530 TB drugs (INH & RIF) in a combination with ZnONPs.
531 MIC values of ZnONPs towards multidrug-resistant (MDR) *Mtb* isolates were found to be
532 higher at 14 μg/ml (Figure 4A). The MBC values for the ZnONPs [17 μg/ml for drug-sensitive
533 H37Rv and 23 μg/ml for multidrug-resistant (MDR) *Mtb* isolates] were further confirmed
534 through agar spread plate method as shown in Supplementary Information (Figure S3,

535 Supplementary Information). Although MDR cells were rendered nonviable at 20 μg/ml of
536 ZnONPs (Figure 4A), based on the data obtained from agar spread plate method (Figure S3,
537 Supplementary Information), for the remaining experiments 23 μg/ml was considered as the
538 MBC for ZnONPs towards MDR *Mtb* cells.
539 In the case of MDR isolates, the anti-TB drugs Moxifloxacin (MXF) and Levofloxacin (LFX),
540 with MICs of 0.125 μg/ml and 0.0625 μg/ml respectively, were compared with the activity of
541 the ZnONPs (Figure 4B). There was a complete loss of viable cell population (blue colour) at
542 LFX (0.25 μg/ml) / MXF (0.125 μg/ml) and their activity was comparable to the effect of
543 ZnONPs at 23 μg/ml (MBC) (Figure 4B). All the cells were rendered non-viable (blue) at
544 concentrations higher than these values for the test compounds. Thus, the antimycobacterial
545 activity of ZnONPs towards MDR *Mtb* isolates was comparable to that of anti-TB drugs MXF
546 and LFX at their respective MIC and higher values. This underscores the potential of ZnONPs
547 as a potent alternative for managing *Mtb* infections
548 Next, the synergistic activity of ZnONPs along with LFX and MXF was evaluated towards
549 MDR *Mtb* isolates (Figures 4C and 4D). A combination of LFX (0.0265 μg/ml)+ ZnONPs (17
550 μg/ml) and LFX (0.125 μg/ml)+ ZnONPs (11 μg/ml) resulted in non-viable cells (blue). A
551 similar observation was made for, MXF (0.031 μg/ml) + ZnONPs (17 μg/ml) and MXF (0.0265
552 μg/ml)+ ZnONPs (11 μg/ml) combinations towards the viability of MDR cells.
553 Thus, both LXF and MXF at their respective MIC and half reduced MIC values could
554 completely abolish mycobacterial cell viability when added together with ZnONPs. In toto,
555 these results suggest that ZnONPs exhibit anti-mycobacterial properties against both H37Rv
556 and MDR *Mtb* cells, indicating their potential utility as an adjunctive therapy in the fight
557 against TB.
558 On the whole, from the results of *in vitro* splicing and Alamar blue assays, ZnONPs-mediated
559 inhibition of mycobacterial growth could be attributed to splicing attenuation induced by

560 interactions between ZnONPs and *Mtb* SufB precursor protein. By targeting essential proteins
561 like the splicing of SufB, ZnONPs are likely to disrupt vital cellular processes in the
562 mycobacteria, leading to growth inhibition and loss of cell viability. To further correlate these
563 events, Alamar blue assay was performed to examine the effect of ZnONPs (0.5 ug/ml to 50
564 ug/ml) on the growth and viability of *Mycobacterium smegmatis* (*M. sm*), in which SufB
565 polypeptide chain lacks an intein sequence (Figure S4, Supplementary Information) [84]. Live
566 viable cells (pink) (Figure S4, Supplementary Information), indicated no effect of ZnONPs (0.5
567 µg/ml to 50 µg/ml) on *M. sm* viability, possibly due to lack of regulatory influence on SufB
568 splicing and cleavage reactions. This provided further evidence to support loss of *Mtb* cell
569 viability (alamar blue assay) as a result of ZnONPs mediated inhibition of *Mtb* SufB splicing
570 and cleavage reactions, although additional mechanisms such as NPs-mediated membrane
571 damage cannot be ruled out.
572 Furthermore, our investigation into combinatorial therapy, integrating lower effective
573 concentrations of known anti-TB drugs alongside ZnONPs, revealed a notable inhibitory effect
574 on the growth and viability of *Mycobacterium tuberculosis* (*Mtb*) cells. Particularly noteworthy
575 was the complete loss of cell viability observed at concentrations half of the MIC values for
576 the individual drugs along with a reduced effective concentration for the NPs (Figures 3C, 3D,
577 4C, and 4D). As shown in Figure 3C, when the concentration for RIF was reduced to 0.5
578 µg/ml (half of MIC), along with 11 µg/ml of ZnONPs, this led to no observable viable growth
579 of H37Rv *Mtb*. Similarly, INH at a concentration of 0.05 ug/ml (half of MIC) completely
580 blocked viability of mycobacterial cells in presence of lower dose of ZnONPs (11 µg/ml)
581 (Figure 3D). In another approach, when RIF and INH were added at their respective MIC (1
582 µg/ml and 0.1 µg/ml respectively), in presence of MIC of ZnONPs (5 µg/ml), no viable cells
583 were observed (Figures 3C, 3D). Similarly, in the case of MDR cells, when LFX and MXF
584 were added at their MIC (0.125 and 0.0625 µg/ml respectively), [85–87] a reduction for ZnONPs

MIC occurred from 14 ug/ml to 0.5 ug/ml, with no growth observed at 11 µg/ml (Figures 4C, 4D).

This strategy demonstrates the potential to achieve significant inhibition of H37Rv as well MDR *Mtb* cells at markedly lower concentrations of conventional anti-TB drugs, with the potential to mitigate the cytotoxic effects associated with prolonged drug administration. The observed synergy between lower doses of existing drugs and ZnONPs presents a promising avenue for enhancing the efficacy of TB management while minimizing potential adverse effects.

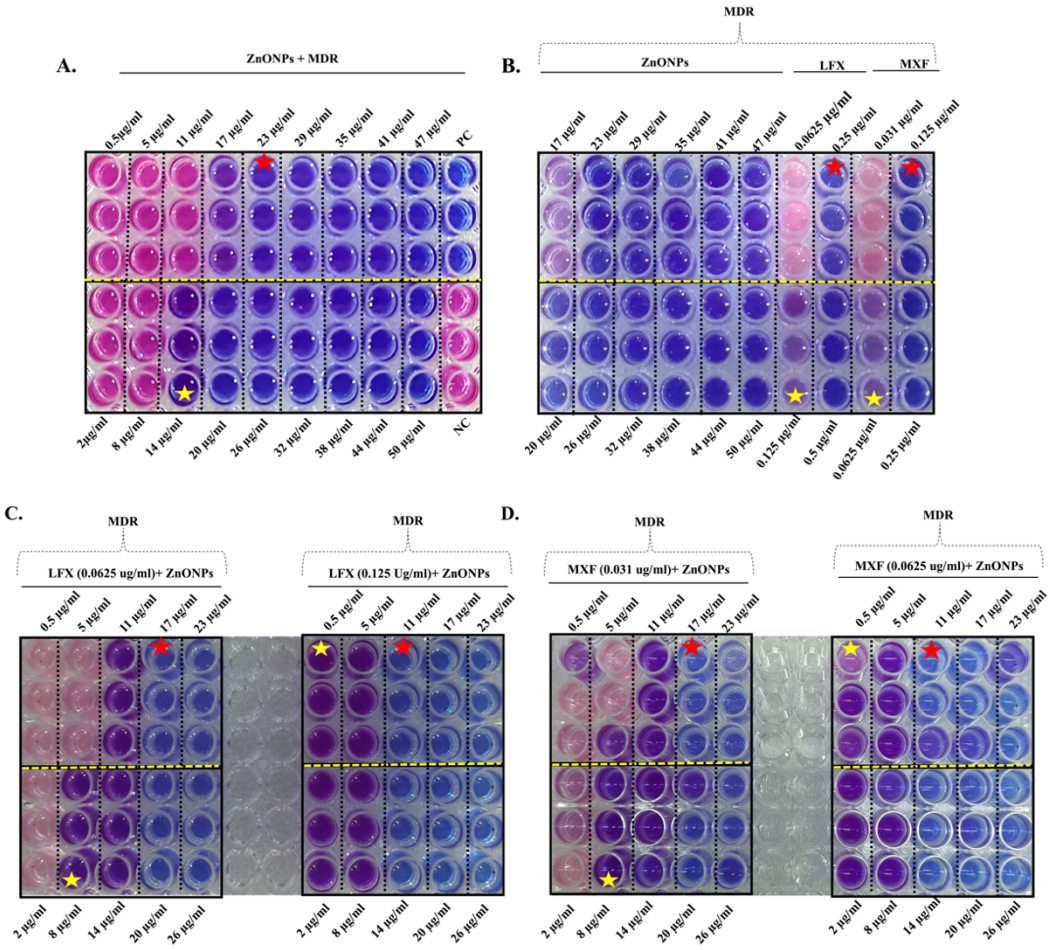

Figure 4. Alamar blue assay to determine the MIC of ZnONPs towards MDR *Mtb* cells. **(A)** Mycobacterial cells were incubated in a 96 well plate, in presence of varied concentrations (0.5 to 50 µg/ml) ZnONPs for 14 days, followed by addition of Alamar Blue reagent. Further incubation at 37ºC for 24 hours, led to colour change in the wells. MIC of ZnONPs was identified as 14 µg/ml where

613 transition of blue to purple colour occurred suggesting partial loss of cell viability among the cells. In
614 contrast, persistence of a blue colour due to complete loss of viable cell population was seen at 23 µg/ml
615 of ZnONPs. Pink cells refer to healthy viable cells resisting inhibitory effect of ZnONPs. **(B)**
616 Comparison of the activity of anti-TB drugs; Levofloxacin (LFX) & Moxifloxacin (MXF) and varied
617 concentration of ZnONPs. All the cells were rendered non-viable (blue) at a concentration of 23 µg/ml
618 for the ZnONPs and in presence of LFX (0.25 µg/ml), MXF (0.125 µg/ml) and at higher concentration.
619 The MIC for LFX & MXF as shown in this study coincided with the known values of 0.125 and 0.0265
620 µg/ml respectively [86]**.** Synergistic activity of ZnONPs and anti-TB drugs; **(C)** LFX & **(D)** MXF. 10^6
621 CFU of bacterial cells were grown in presence of varied concentrations of ZnONPs and the drugs. A
622 combination of LFX (0.0625 µg/ml) + ZnONPs (17 µg/ml) & LFX (0.126 µg/ml) + ZnONPs (11 µg/ml)
623 successfully yielded non-viable cells (blue). Likewise, MXF (0.031 µg/ml) + ZnONPs (17 µg/ml) &
624 MXF (0.0625 µg/ml) + ZnONPs (11 µg/ml) combinations resulted in non-proliferating cells (blue). Red
625 stars- complete loss of viability & Yellow stars- partial loss of viable cells (purple) at a lower
626 concentration of NPs. MDR: Multidrug-resistant, LFX: Levofloxacin, MXF: Moxifloxacin
627

628 *3.4 ZnONPs exhibit bactericidal effects on drug-sensitive and MDR Mtb* cells

629 Current work validated the interaction between ZnONPs and *Mtb* SufB, which influenced cell
630 viability, and this can be attributed to the production of a non-functional SufB protein via
631 splicing inhibition, a vital component for *Mtb* survival [11,13]. The observed decrease in viability
632 could also be associated with a cumulative effect of mycobacterial membrane damage activity
633 induced by ZnONPs [42]. To substantiate this hypothesis, we performed a scanning electron
634 microscopy (SEM) analysis, employing various ZnONPs concentrations; a lower concentration
635 of 0.5 µg/ml, two effective concentrations of 17 and 23 µg/ml (MBC for ZnONPs towards
636 H37Rv and MDR *Mtb* cells), and 50 µg/ml, the upper limit for toxicity. These concentrations
637 were selected to cover the effective range of ZnONPs for *in vitro* splicing studies, and MBC
638 values identified by Alamar blue assay & spread plate method.

639 Treatment with ZnONPs at a concentration of 0.5 µg/ml induced minor alterations in the
640 bacterial morphology. However, exposure to concentrations of 17 µg/ml, 23 µg/ml, and 50
641 µg/ml led to extensive membrane disruption, cell-fusion, and cytoplasmic leakage

642 accompanied by a complete loss of cellular morphology (Figures 5A and 5B). Thus, SEM
643 analysis offers substantial evidence of the membrane-damaging activity of ZnONPs towards
644 H37Rv and MDR *Mtb* isolates. This uniform activity of ZnONPs against both drug-sensitive
645 and MDR *Mtb* cells validates our previous observations on antimycobacterial effectiveness
646 detected via Alamar blue assay. This result is particularly significant in the context of MDR-
647 TB, where conventional antibiotic treatments encounter substantial obstacles.

648

649
650
651
652
653
654
655
656
657
658
659
660
661
662
663
664
665
666
667

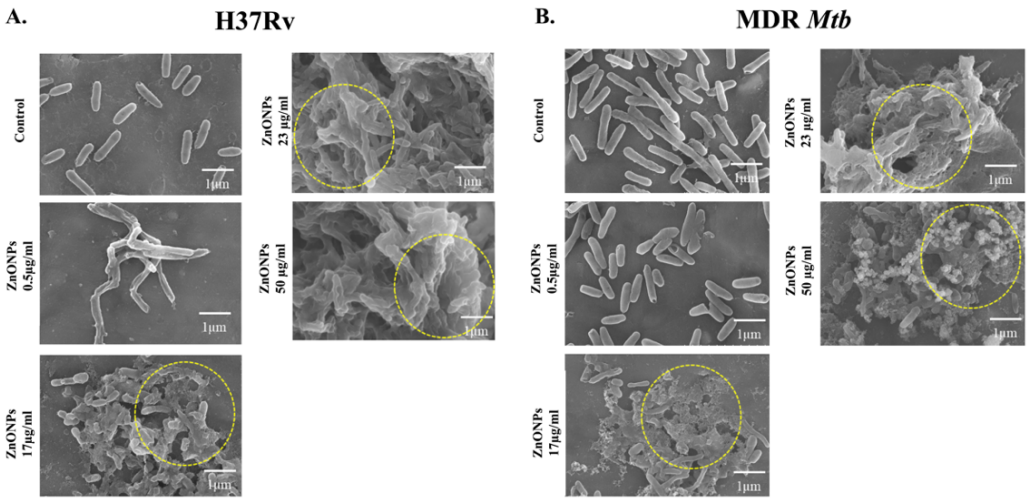

668 **Figure 5. SEM analysis displaying bactericidal role of ZnONPs on *Mycobacterium***
669 ***tuberculosis (Mtb)*** cells **(A)** H37Rv **(B)** MDR *Mtb* isolates. Control (untreated) mycobacterial cells
670 were uniform looking, without any changes in the cell morphology or any evidence of membrane
671 damage. Mild alterations in cellular morphology were noted for both H37Rv, and MDR *Mtb* cells in
672 presence of 0.5 µg/ml of ZnONPs. Dose dependent increase in the severity of cell membrane damage,
673 cell fusion, loss of cellular architecture, were identified among the **(A)** H37Rv and **(B)** MDR *Mtb*
674 isolates, across rest of the ZnONPs test concentration range (17 µg/ml, 23 µg/ml , and 50 µg/ml)
675 (outlined by yellow circles). MDR: Multidrug-resistant *Mtb*

676

677

678

679

680 3.5 *ZnONPs rescue Mtb induced changes in infected mice model*

681 So far, *in vitro* data from this work suggested potent mycobactericidal activity of ZnONPs
682 against H37Rv and MDR *Mtb* isolates, possibly by inhibiting the splicing of essential protein
683 *Mtb* SufB, leading to loss of viability and membrane damage. To further assess this activity in
684 *in vivo* setting, we conducted experiments in mice model.

685 The utilization of *Mtb* H37Ra (H37Rv attenuated strain)-infected mice serves as an established
686 *in vivo* model to evaluate TB infection [88]. Both H37Ra and H37Rv *Mtb* strains are inhibited
687 by similar concentrations of anti-TB drugs as suggested by an earlier work [89]. Hence, the
688 efficacy of ZnONPs-drug combination and recovery from the infection was further tested in
689 H37Ra-infected mice.

690 BALB/6 mice were infected with *Mtb* H37Ra; 1X PBS (placebo), ZnONPs, and drug (RIF)
691 administration commenced four days post-infection and continued for a total of seven days,
692 with mice sacrificed on day 18 post-infection for subsequent histopathological and bacterial
693 burden analysis (experimental design elucidated in Figure 6A). Administration of RIF dosages
694 is based on earlier works published elsewhere [90,91]. Our findings revealed a strong anti-*Mtb*
695 effect of ZnONPs, as evidenced by the analysis of the gross morphology of spleen,
696 histopathological and bacterial burden outcomes.

697 A significant splenomegaly was observed in the infected mouse which had received 1X PBS
698 as a placebo following infection with H37Ra strain [92–96]. Resistance to this morphological
699 effect was observed in infected mice, receiving RIF (15 mg/kg), ZnONPs (26 and 50 µg/ml),
700 RIF (10 mg/kg) + ZnONPs (26 µg/ml), and RIF (10 mg/kg) + ZnONPs (50 µg/ml). The
701 splenomegaly following H37Ra infection in the aforementioned experimental groups was
702 rescued significantly when ZnONPs was given as a solo treatment at concentration of 26 µg/ml,
703 and 50 µg/ml. The efficacy of RIF at 15 mg/kg was similar to a combination containing a
704 reduced dosage of RIF at 10 mg/kg along with ZnONPs (26 µg/ml, and 50 µg/ml), where a

complete rescue from splenomegaly was seen; comparable to the normal sized spleen in healthy cage control mouse (Figure 6B). Likewise, a substantial reduction in mycobacterial load in lungs and spleen were observed in similarly treated mice groups, emphasizing the superior anti-TB activity of the ZnONPs/RIF combination (Figures 6C and 6D). Bacterial loads were equivalently attenuated when RIF was administered solo at 15 mg/kg or in combination (RIF 10 mg/kg + ZnONPs 26 µg/ml or RIF 10 mg/kg + ZnONPs 50 µg/ml) at a lower concentration. This highlights the synergistic activity of these anti-*Mtb* compounds displaying a higher potential to manage mycobacterial infection.

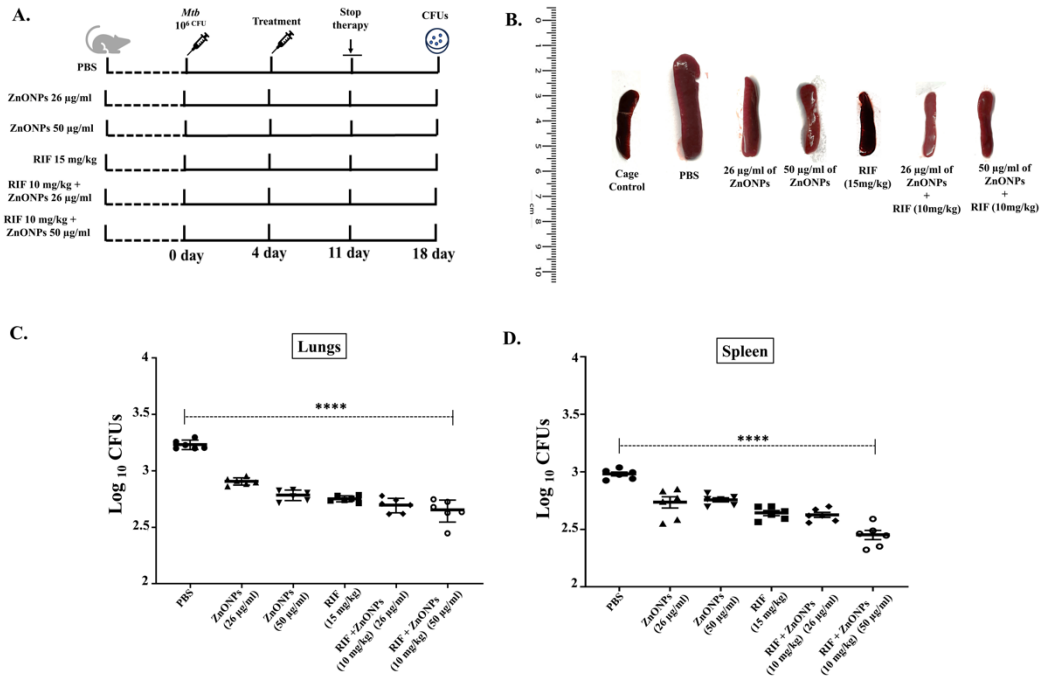

Figure 6. *In vivo* antimycobacterial effects of ZnONPs in H37Ra infected mice model. (A) Schematic representation of the experimental design in BALB/c mice (n = 6 in each group). Mice were infected with H37Ra*;* 1X PBS (placebo)*,* NPs and drug administration commenced four days post-infection and continued for a total of seven days, with mice sacrificed on day 18th post-infection. **(B)** Significant splenomegaly was noticed in the infected mouse which had received 1X PBS only. This was not observed in the infected mice, who were given RIF (15 mg/kg), RIF (10 mg/kg) + ZnONPs (26 µg/ml), and RIF (10 mg/kg) + ZnONPs (50 µg/ml), where the spleen size was comparable to the normal sized spleen in healthy cage control mouse. The splenomegaly was partially rescued in mice who had

733 received ZnONPs (26 or 50 µg/ml) alone. Bacterial burden in the **(C)** lungs, and **(D)** spleen of the
734 infected mice was determined by plating the organ lysate on the 7H10 plates after treatment with
735 ZnONPs or 1XPBS for 7 days. Significant reduction in mycobacterial loads was observed in mice
736 groups treated with a combination therapy, emphasizing the superior anti-TB activity of the ZnONPs-
737 RIF combination. Data are presented as mean ± 1 SD ($p>0.0001$) from values obtained from (n=6) mice.
738

739 Next, histopathological examination of infected lungs and spleen tissues provided additional
740 evidence for the anti-mycobacterial efficacy of ZnONPs. Lungs sections from cage control
741 healthy mice displayed clear lung fields without any evidence of inflammation [Figure 7A(a)].
742 Infected mice group administered with 1XPBS displayed distinct pathological changes in the
743 lungs with noticeable inflammatory infiltrates, indicative of infection induced immune
744 response [Figure 7A(b)] [97]. When administered individually, ZnONPs (26 µg/ml), ZnONPs (50
745 µg/ml), and RIF (15 mg/kg) caused a partial reduction in inflammatory cells within the lungs
746 [Figures 7A(c), (d), and (e)]. On the contrary, mice treated with a combination of ZnONPs (26
747 µg/ml) + RIF (10 mg/kg) and ZnONPs (50 µg/ml) + RIF (10 mg/kg) respectively,
748 demonstrated no inflammatory infiltrations, suggesting their superior anti-mycobacterial
749 action ([Figures 7A(f), and (g)].
750 Similarly, inflammatory changes were noted within the white pulp of the infected splenic
751 tissue, which is a critical component of the organ's immune function [98]. Healthy mice from the
752 cage control group exhibited normal spleen histology with clear differentiation into white and
753 red pulps [Figure 7B(a)] [99] whereas, infected mice treated with 1XPBS, depicted rich
754 inflammatory infiltrates obscuring normal spleen histology [Figure 7B(b)] [100]. A partial
755 reduction in inflammation was observed, along with a restoration of the white and red pulp
756 structures in the spleen of the mice treated with ZnONPs (26 µg/ml), and ZnONPs (50 µg/ml),
757 respectively [Figures 7B(c), and (d)]. Notably, in the mice group that received RIF (15 mg/kg)
758 alone or combination therapy [ZnONPs (26 µg/ml) + RIF (10 mg/kg) and ZnONPs (50 µg/ml)
759 + RIF (10 mg/kg)], there were no inflammatory infiltrations, and distinct white and red pulp

structures were evident ([Figures 7B(e), (f), and (g)]. Hence, the efficacy of the combinatorial approach with a reduced dose of RIF (10 mg/kg) was similar to RIF solo therapy at a higher concentration (15 mg/kg).

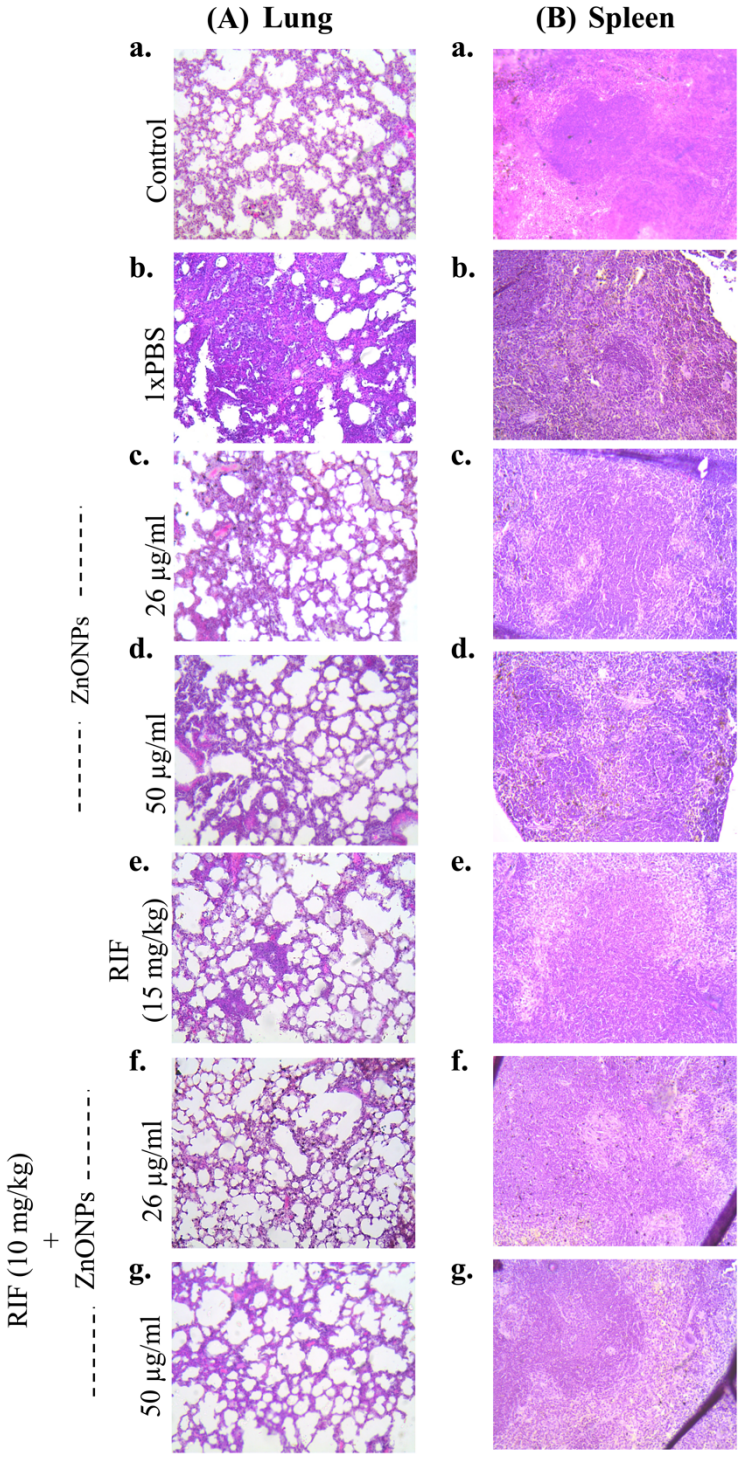

786

787 **Figure 7. Histopathology of lungs and spleen from H37Ra infected mice (H37Rv attenuated**
788 **strain), comparing the efficacy of ZnONPs, RIF, and ZnONPs-RIF combinations. (A)** Lungs
789 sections are stained by H&E staining and processed for visualization by microscopy. **(a)** Histology of
790 uninfected lungs in healthy control mice. **(b-e)** represent tissue sections from infected mice who have
791 received different solo treatments, (**b)** 1XPBS exhibiting prominent aggregates of inflammatory cells;
792 (**c)** 26 ug/ml of ZnONPs, **(d)** 50 ug/ml of ZnONPs , and **(e)** RIF 15 mg/kg displaying partial reduction
793 in immune cells infiltrates; **(f)** RIF (10 mg/kg) + ZnONPs (26 ug/ml), and **(g)** RIF (10 mg/kg) + ZnONPs
794 (50 ug/ml) represent no inflammatory changes and restoration of normal lungs histology. **(B)** Tissue
795 sections from spleen are stained by H&E staining and processed for visualization by microscopy. **(a)**
796 Histology of spleen in uninfected healthy control mice showing well differentiated white and red pulp
797 structures. **(b-e)** represent tissue sections from infected mice who have received different solo
798 treatments; **(b)** 1XPBS exhibiting heavy immune cell aggregates obliterating white and red pulps; **(c)**
799 26 ug/ml of ZnONPs, **(d)** 50 ug/ml of ZnONPs, are displaying partial rescue from inflammatory
800 infiltrates; **(e)** RIF 15 mg/kg**, (f)** RIF (10 mg/kg) + ZnONPs (26 ug/ml), and **(g)** RIF (10 mg/kg) +
801 ZnONPs (50 ug/ml)**,** either of these treatments when given to infected mice, restored normal spleen
802 histology with no evidence of inflammation. Images represent different experimental groups of mice
803 visualized under 10X magnification. H&E- Hematoxylin and eosin staining; RIF- Rifampicin
804

805 These observations support a potential therapeutic effect of the ZnONPs against
806 *Mycobacterium tuberculosis* (*Mtb*). A concurrent mode of action combining, SufB splicing
807 inhibition by ZnONPs along with inhibition of bacterial RNA polymerase due to RIF, and
808 ZnONPs mediated membrane damage, possibly facilitates complete resolution of inflammation
809 restoring normal spleen and lung histology [101]. Taken together, these findings provide a strong
810 foundation for further investigation into the mechanisms underlying the *in vivo* anti-
811 mycobacterial activity of ZnONPs towards drug-sensitive as well as MDR TB. Additionally,
812 long-term studies evaluating the safety and sustained efficacy of ZnONPs will be crucial for
813 assessing their potential as a viable therapeutic option.

814

815

816

4. Conclusion

One of the major milestones of the United Nations Sustainable Development Goals (SDGs) is to end TB by 2030 [102]. Besides aiming for accessible patient care with attenuated hospitalization rate, WHO also calls for "adoption to innovations" in TB management [2]. The escalating challenge of drug-resistant TB, necessitates the exploration of novel therapeutic strategies such as nanomedicine. Current work investigates into the mycobactericidal role of the ZnONPs against both H37Rv *Mtb* strain and MDR *Mtb* isolates, by blocking generation of crucial SufB protein via intein splicing inhibition .

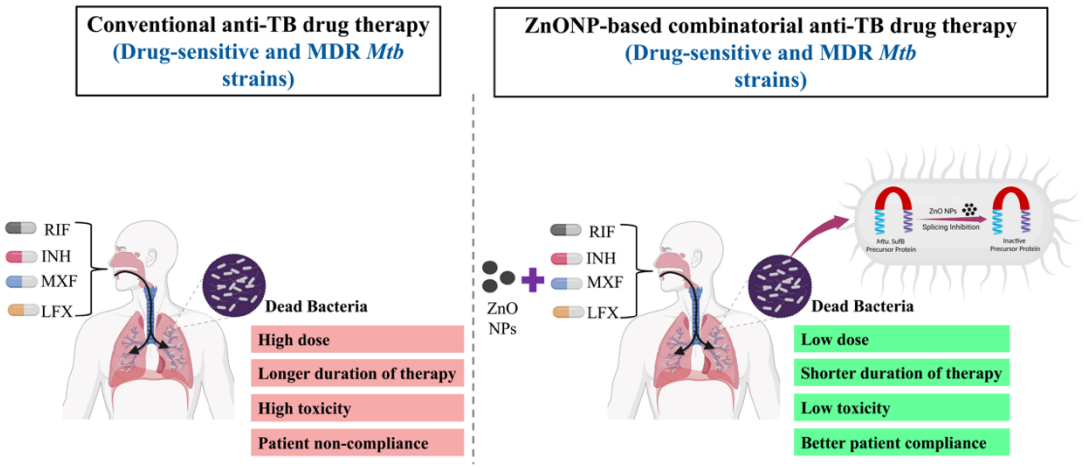

Figure 8. Schematic diagram illustrating the proposed mechanism for higher efficacy of combination therapy in managing drug-susceptible and MDR TB, contrasting with conventional drug therapy. ZnONPs and RIF/INH or MXF/LFX combination exhibits superior therapeutic potential possibly via a dual approach: targeting the mycobacterial viability by splicing regulation to inhibit generation of essential protein SufB, further supported by the potent antimycobacterial action of anti-TB drugs. Multidrug-resistant (MDR), Rifampicin (RIF), Isoniazid (INH), Moxifloxacin (MXF), Levofloxacin (LFX).

A series of *in vitro* experiments, encompassing Bradford assays, UV-Visible spectroscopy, and Transmission Electron Microscopy (TEM), have collectively substantiated the interaction between the ZnONPs and the SufB protein. This interaction has been observed to induce a

845 significant alteration in the *Mtb* viability possibly due to loss of protein's biological activity.
846 The Alamar Blue assay and Scanning Electron Microscopy (SEM) analysis further elucidated
847 the bactericidal effects of the ZnONPs on H37Rv and MDR *Mtb* cells, which was correlated to
848 the inhibitory effects of the ZnONPs on splicing and cleavage reactions of SufB precursor
849 protein. While SEM confirmed extensive mycobacterial membrane damage, the Alamar blue
850 assay highlighted the superior efficacy of a combination therapy (ZnONPs-INH/RIF &
851 ZnONPs-LFX/MXF), where the effective dosage of the anti-TB drugs were reduced by half
852 towards both drug-sensitive strain and MDR *Mtb* isolates [82,83,85–87]. Next, *in vivo* experiments
853 in infected mice model, validated substantial anti-mycobacterial activity of ZnONPs-RIF
854 combination against the *Mtb* H37Ra strain. These collective findings underscore the potential
855 of ZnONPs as a promising additive along with existing anti-TB drugs in the fight against
856 tuberculosis.
857 Herein, we propose a dual mode of action for this ZnONPs-based combinatorial approach:
858 ZnONPs can significantly influence mycobacterial viability by complete blockage of splicing
859 and cleavage reactions to inhibit generation of essential protein SufB, further supported by the
860 potent antimycobacterial action of anti-TB drugs (Figure 8). Since eukaryotes such as humans
861 lack intein sequences, and microbial intein sequences resist mutations, targeted drug
862 development strategy aiming splicing regulation of critical proteins have been proposed as
863 novel mechanisms to manage drug-resistant infections [103]. Current study also highlights the
864 reduction in the effective dosage for the anti-TB drugs in combination with ZnONPs, that will
865 address caveats such as drug toxicity. However, further research and clinical trials will be
866 essential to validate the safety and efficacy of ZnONPs as a potential supportive treatment
867 option for the infected patients.
868 This study's uniqueness lies in its innovative approach that demonstrated bactericidal efficacy
869 against both drug-sensitive and MDR *Mtb* isolates, as a significant improvement over earlier

research. Furthermore, the inhibition of SufB splicing by ZnONPs provides a new mechanism for managing TB, distinct from existing treatments. Additionally, the reduced dose of RIF/INH and MXF/LFX when combined with ZnONPs may lead to fewer adverse effects and improved patient compliance, especially addressing concerns during extended treatment periods (as in case of disseminated TB). Moreover, the potential toxicity of ZnONPs can be further eliminated by obtaining NPs via green synthesis routes [104,105]. Howbeit, future research should focus on clinical trials to validate these findings and explore the long-term benefits and safety of this combinatorial approach. Current study addresses the growing issue of drug-resistant TB by exploring a new therapeutic approach that can have a significant contribution to the field of TB research and management. Higher efficacy along with lower drug dosage and probable shorter treatment duration may have a positive impact on the overall health cost, facilitating global effort to fight against TB.

Author contributions

Deepak Kumar Ojha: Conceptualization, Resources, Data curation, Formal Analysis, Validation, Visualization, Methodology, Writing—original draft, Writing—review & editing; Ashwaria Mehra: Resources, Data curation, Funding acquisition, Validation, Methodology, Writing—review & editing; Sunil Swick Rout: Resources, Data curation, Software, Validation, Visualization; Sidhartha Giri: Resources, Validation, review & editing; Sasmita Nayak: Conceptualization, Resources, Data curation, Formal Analysis, Supervision, Funding acquisition, Validation, Investigation, Visualization, Methodology, Writing—original draft, Project administration, Writing—review & editing.

Conflicts of interest

There are no conflicts to declare

894 **Data Availability**

895 The data underlying the present article are available in the article and in its online
896 Supplementary Information.

897 **Acknowledgements**

898 The plasmids used in the present study are borrowed from Prof. Marlene Belfort's Lab, SUNY,
899 Albany, NY, U.S.A. Our sincere gratitude to the Central Instrumentation facility (CIF) at
900 OUAT (Odisha University of Agriculture & Technology), Bhubaneswar and Dr. S.K Dash for
901 his help in conducting SEM analysis at OUAT Bhubaneswar. We thank to Dr. Sravan Kumar
902 for his help in conducting TEM analysis at the Central Institute of Petrochemicals Engineering
903 and Technology (CIPET), Bhubaneswar. We extend our gratitude to Dr. Sidhartha Giri for
904 providing access to the Biosafety Level 3 (BSL3) laboratory facility at ICMR-RMRC,
905 Bhubaneswar, for smooth conductance of mycobacterial experiments.

906 **Ethics Statement**

907 The animal study was reviewed and approved/recommended by the IAEC of Kalinga Institute
908 of Industrial technology Deemed to be University (KIIT-DU), Bhubaneswar, Odisha.
909 (Approval No. KSBT/IAEC/2023/2/14.2)

910 **Funding**

911 This work is supported by Indian Council of Medical Research (ICMR), India (ICMR Project
912 ID: IIRP-2023-7834/F1). A.M. is supported by INSPIRE fellowship
913 (DST/INSPIRE/03/2021/002800/IF 190921); INSPIRE Division, DST, Government of India.

914

915 **Abbreviations**

Ab, antibody; ANOVA, Analysis of Variance; CC , C-terminal cleavage product; IB , inclusion bodies; IPTG, isopropyl β-d-1-thiogalactopyranoside; I, intein; CC, C-terminal cleavage; P, precursor; LE, ligated extein; MDR, multidrug resistant; DS, Drug sensitive ; DR, Dug resistance; *Mtb*, *Mycobacterium tuberculosis*; NC, N-terminal cleavage product; NE, N-extein; Ni-NTA, nickel-nitrilotriacetic acid; PAGE, polyacrylamide gel electrophoresis; PVDF, polyvinylidene fluoride; SI, splicing inactive; SDS, sodium dodecyl sulfate; SEM, Scanning Electron Microscope; SUF, Mobilization of Sulphur; TB, Tuberculosis; TCEP.HCl, tris 2-carboxyl ethyl phosphine. Hydrochloric acid; TNB, 2-nitro-5-thiobenzoic acid; UV–Vis, UV–visible spectroscopy; WT, wild-type; NP, Nanoparticle; ZnO, zinc oxide; H&E; Hematoxylin and eosin.

References

1 D. R. Silva, F. C. de Queiroz Mello and G. B. Migliori, *Jornal Brasileiro de Pneumologia*, 2020, **46**, e20200027.

2 G. W. H. Organization, 2023.

3 K. J. Seung, S. Keshavjee and M. L. Rich, *Cold Spring Harb Perspect Med*, DOI:10.1101/cshperspect.a017863.

4 A. Prasanna and V. Niranjan, *Bioinformation*, 2019, **15**, 261–268.

5 S. N. Goossens, S. L. Sampson and A. Van Rie, *Clin Microbiol Rev*, DOI:10.1128/CMR.00141-20.

6 K. H. Alzahabi, O. Usmani, T. K. Georgiou, M. P. Ryan, B. D. Robertson, T. D. Tetley and A. E. Porter, *Emerg Top Life Sci*, 2021, 4.

7 S. Panda, A. Nanda, N. Sahu, D. K. Ojha, B. Pradhan, A. Rai, A. R. Suryawanshi, N. Banavali and S. Nayak, *Biosci Rep*, DOI:10.1042/BSR20212207.

8 S. Panda, A. Nanda, S. S. Nasker, A. Mehra, D. K. Ojha, P. S. Mohanty and S. Nayak, *Clin Sci*, DOI:10.1042/CS20230307.

9 O. Novikova, P. Jayachandran, D. S. Kelley, Z. Morton, S. Merwin, N. I. Topilina and M. Belfort, *Mol Biol Evol*, DOI:10.1093/molbev/msv271.

10 F. Wayne Outten, *Biochim Biophys Acta Mol Cell Res*, 2015, 1853.

11 G. Huet, M. Daffé and I. Saves, *J Bacteriol*, 2005, **187**, 6137–6146.

12 H. K. Chahal, Y. Dai, A. Saini, C. Ayala-Castro and F. W. Outten, *Biochemistry*, DOI:10.1021/bi901518y.

13 G. Huet, J. P. Castaing, D. Fournier, M. Daffé and I. Saves, *J Bacteriol*, 2006, **188**, 3412–3414.

14 K. W. Jayawardana, H. S. N. Jayawardena, S. A. Wijesundera, T. De Zoysa, M. Sundhoro and M. Yan, *Chemical Communications*, DOI:10.1039/c5cc04251h.

15 P. V Mohanan, V. G. Reshma, S. Syama, S. Sruthi, S. C. Reshma and N. S. Remya, *Curr Drug Metab*, DOI:10.2174/1389200218666170925122201.

16 M. Vallet-Regí, B. González and I. Izquierdo-Barba, *Int J Mol Sci*, 2019, 20.

17 A. C. Anselmo and S. Mitragotri, *Bioeng Transl Med*, DOI:10.1002/btm2.10003.

18 G. T. Tietjen and W. M. Saltzman, *Sci Transl Med*, DOI:10.1126/scitranslmed.aad6645.

19 A. Gallud, H. Líbalová and B. Fadeel, *Nanomedicine*, DOI:10.2217/nnm.15.79.

20 T. Sun, Y. S. Zhang, B. Pang, D. C. Hyun, M. Yang and Y. Xia, *Angewandte Chemie - International Edition*, 2014, 53.

21 J. N. BARRY and A. A. VERTEGEL, *Nano Life*, DOI:10.1142/s1793984413430010.

22 S. J. Park, *Int J Nanomedicine*, 2020, 15.

23 S. R. Saptarshi, A. Duschl and A. L. Lopata, *J Nanobiotechnology*, DOI:10.1186/1477-3155-11-26.

24 D. Peer, J. M. Karp, S. Hong, O. C. Farokhzad, R. Margalit and R. Langer, *Nat Nanotechnol*, 2007, 2.

25 K. K. Jain, *Clinica Chimica Acta*, 2005, 358.

26 Y. Barenholz, *Journal of Controlled Release*, 2012, 160.

27 X. Hou, T. Zaks, R. Langer and Y. Dong, *Nat Rev Mater*, 2021, 6.

28 J. Theron, J. A. Walker and T. E. Cloete, *Crit Rev Microbiol*, 2008, 34.

29 A. Gogos, K. Knauer and T. D. Bucheli, *J Agric Food Chem*, DOI:10.1021/jf302154y.

30 J. Mou, Z. Liu, J. Liu, J. Lu, W. Zhu and D. Pei, *Drug Deliv*, DOI:10.1080/10717544.2019.1571121.

31 C. Pushpalatha, J. Suresh, V. S. Gayathri, S. V. Sowmya, D. Augustine, A. Alamoudi, B. Zidane, N. H. Mohammad Albar and S. Patil, *Front Bioeng Biotechnol*, 2022, 10.

32 X. Li, C. Yuan, Q. Chen, Q. Xue, J. Mou and P. Wang, *Med Oral Patol Oral Cir Bucal*, 2023, **28**, e487–e495.

33 Y. Wang, H. Hua, W. Li, R. Wang, X. Jiang and M. Zhu, *J Dent*, 2019, **80**, 23–29.

34 C. Petchthanasombat, T. Tiensing and P. Sunintaboon, *J Colloid Interface Sci*, 2012, **369**, 52–57.

35 S. Raha and M. Ahmaruzzaman, *Nanoscale Adv*, 2022, 4.

36 United States Food and Drug Administration, Food and Drugs; Part-182 Substances Generally Recognized as Safe, https://www.accessdata.fda.gov/scripts/cdrh/cfdocs/cfcfr/cfrsearch.cfm?fr=182.8991, (accessed 19 June 2024).

37 J. W. Rasmussen, E. Martinez, P. Louka and D. G. Wingett, *Expert Opin Drug Deliv*, 2010, 7.

38 E. M. El-Diasty, M. A. Ahmed, N. Okasha, S. F. Mansour, S. I. El-Dek, H. M. Abd El-Khalek and M. H. Youssif, *ANTIFUNGAL ACTIVITY OF ZINC OXIDE NANOPARTICLES AGAINST DERMATOPHYTIC LESIONS OF CATTLE*, 2013, vol. 23.

39 S. Jha, R. Rani and S. Singh, *J Inorg Organomet Polym Mater*, 2023, 33.

40 M. Heidary, S. Z. Bostanabad, S. M. Amini, A. Jafari, M. G. Nobar, A. Ghodousi, M. Kamalzadeh and D. Darban-Sarokhalil, *Infect Drug Resist*, DOI:10.2147/IDR.S221408.

41 W. Lin, S. Fan, K. Liao, Y. Huang, Y. Cong, J. Zhang, H. Jin, Y. Zhao, Y. Ruan, H. Lu, F. Yang, C. Wu, D. Zhao, Z. Fu, B. Zheng, J. F. Xu and J. Pi, *Front Cell Infect Microbiol*, DOI:10.3389/fcimb.2022.1074533.

42 A. J. Caron, I. J. Ali, M. J. Delgado, D. Johnson, J. M. Reeks, Y. M. Strzhemechny and S. M. McGillivray, *Front Microbiol*, 2024, **15**, 1394078.

43 S. V. Gudkov, D. E. Burmistrov, D. A. Serov, M. B. Rebezov, A. A. Semenova and A. B. Lisitsyn, *Front Phys*, 2021, 9.

44 P. Sun, S. Ye, S. Ferrandon, T. C. Evans, M. Q. Xu and Z. Rao, *J Mol Biol*, DOI:10.1016/j.jmb.2005.09.039.

45 B. W. Poland, M. Q. Xu and F. A. Quiocho, *Journal of Biological Chemistry*, DOI:10.1074/jbc.275.22.16408.

46 L. Zhang, Y. Zheng, Z. Xi, Z. Luo, X. Xu, C. Wang and Y. Liu, *Mol Biosyst*, DOI:10.1039/b903144h.

47 P. Van Roey, B. Pereira, Z. Li, K. Hiraga, M. Belfort and V. Derbyshire, *J Mol Biol*, DOI:10.1016/j.jmb.2006.12.050.

48 S. Panda, A. Nanda, S. S. Nasker, D. Sen, A. Mehra and S. Nayak, *Biochimie*, 2021, 185.

49 D. Woods, S. Vangaveti, I. Egbanum, A. M. Sweeney, Z. Li, V. Bacot-Davis, D. S. Lesassier, M. Stanger, G. E. Hardison, H. Li, M. Belfort and C. W. Lennon, *mBio*, DOI:10.1128/mBio.01403-20.

50 R. Afarin, F. Ahmadpour, M. Hatami, S. Monjezi and S. Igder, *Heliyon*, 2024, **10**, e31925.

51 Q. Lin, Y. Jing, C. Yan, X. Chen, Q. Zhang, X. Lin, Y. Xu and B. Chen, *Int J Nanomedicine*, 2024, **Volume 19**, 5381–5395.

52 B. Naiel, M. Fawzy, A. E. D. Mahmoud and M. W. A. Halmy, *Sci Rep*, 2024, **14**, 13459.

53 A. Nanda, S. S. Nasker, A. K. Kushwaha, D. K. Ojha, A. K. Dearden, S. K. Nayak and S. Nayak, *Front Bioeng Biotechnol*, DOI:10.3389/fbioe.2021.773303.

54 E. Suhartono, I. Thalib, I. Aflanie, Z. Noor and R. Idroes, in *IOP Conference Series: Materials Science and Engineering*, 2018, vol. 350.

55 P. K. Grzyska, R. P. Hausinger and D. A. Proshlyakov, *Anal Biochem*, 2010, **399**, 64–71.

56 J. Saikia, M. Yazdimamaghani, S. P. Hadipour Moghaddam and H. Ghandehari, *ACS Appl Mater Interfaces*, DOI:10.1021/acsami.6b09950.

57 G. Su, H. Jiang, B. Xu, Y. Yu and X. Chen, *Mol Pharm*, DOI:10.1021/acs.molpharmaceut.8b00612.

58 A. M. Clemments, C. Muniesa, C. C. Landry and P. Botella, *RSC Adv*, 2014, **4**, 29134–29138.

59 A. Nanda, S. S. Nasker, A. K. Kushwaha, D. K. Ojha, A. K. Dearden, S. K. Nayak and S. Nayak, *Front Bioeng Biotechnol*, 2021, **9**, 773303.

60 A. Sasidharan, J. E. Riviere and N. A. Monteiro-Riviere, *J Mater Chem B*, 2015, **3**, 2075–2082.

61 K. Friedel, M. A. Popp, J. C. J. Matern, E. M. Gazdag, I. V. Thiel, G. Volkmann, W. Blankenfeldt and H. D. Mootz, *Chem Sci*, DOI:10.1039/C8SC01074A.

62 L. Zhang, Y. Zheng, B. Callahan, M. Belfort and Y. Liu, *Journal of Biological Chemistry*, DOI:10.1074/jbc.M110.171124.

63 K. V. Mills, B. M. Lew, S. Q. Jiang and H. Paulus, *Proc Natl Acad Sci U S A*, DOI:10.1073/pnas.95.7.3543.

64 K. V. Mills and H. Paulus, *Journal of Biological Chemistry*, DOI:10.1074/jbc.M011149200.

65 J. P. Gangopadhyay, S. qin Jiang and H. Paulus, *Anal Chem*, DOI:10.1021/ac020756b.

66 H. Chan, C. S. Pearson, C. M. Green, Z. Li, J. Zhang, G. Belfort, A. Shekhtman, H. Li and M. Belfort, *Journal of Biological Chemistry*, DOI:10.1074/jbc.M116.747824.

67 K. Punjabi, S. Mehta, R. Chavan, V. Chitalia, D. Deogharkar and S. Deshpande, *Front Microbiol*, DOI:10.3389/fmicb.2018.02207.

68 W. Zhou, B. Yang, Y. Zou, K. Rahman, X. Cao, Y. Lei, R. Lai, Z. F. Fu, X. Chen and G. Cao, *Front Microbiol*, DOI:10.3389/fmicb.2021.658637.

69 E. M. Longhin, N. El Yamani, E. Rundén-Pran and M. Dusinska, *Frontiers in Toxicology*, DOI:10.3389/ftox.2022.981701.

70 C. Mahendra, M. N. Chandra, M. Murali, M. R. Abhilash, S. B. Singh, S. Satish and M. S. Sudarshana, *Process Biochemistry*, DOI:10.1016/j.procbio.2019.10.020.

71 S. Sharma, E. Gelman, C. Narayan, D. Bhattacharjee, V. Achar, V. Humnabadkar, V. Balasubramanian, V. Ramachandran, N. Dhar and N. Dinesh, *Antimicrob Agents Chemother*, DOI:10.1128/AAC.03205-14.

72 S. Panda, T. K. Rout, A. D. Prusty, P. M. Ajayan and S. Nayak, *Advanced Materials*, DOI:10.1002/adma.201702149.

73 L. Abarca-Cabrera, P. Fraga-García and S. Berensmeier, *Biomater Res*, 2021, 25.

74 C. Eisner, H. Ow, T. Yang, Z. Jia, E. Dimitriadis, L. Li, K. Wang, J. Briggs, M. Levine, J. Schnermann and M. G. Espey, *J Appl Physiol*, DOI:10.1152/japplphysiol.01068.2011.

75 G. Yan, Y. Huang, Q. Bu, L. Lv, P. Deng, J. Zhou, Y. Wang, Y. Yang, Q. Liu, X. Cen and Y. Zhao, *J Environ Sci Health A Tox Hazard Subst Environ Eng*, DOI:10.1080/10934529.2012.650576.

76 A. M. Florea, F. Splettstoesser and D. Büsselberg, *Toxicol Appl Pharmacol*, DOI:10.1016/j.taap.2007.01.022.

77 R. V.G. and M. P.V., *Colloids Surf B Biointerfaces*, DOI:10.1016/j.colsurfb.2017.05.069.

78 M. Kokkinopoulou, J. Simon, K. Landfester, V. Mailänder and I. Lieberwirth, *Nanoscale*, DOI:10.1039/c7nr02977b.

79 G. Huet, M. Daffé and I. Saves, *J Bacteriol*, DOI:10.1128/JB.187.17.6137-6146.2005.

80 V. Valdiglesias, A. Alba-González, N. Fernández-Bertólez, A. Touzani, L. Ramos-Pan, A. T. Reis, J. Moreda-Piñeiro, J. Yáñez, B. Laffon and M. Folgueira, *Int J Mol Sci*, DOI:10.3390/ijms241512297.

81 B. N. Patil and T. C. Taranath, *Int J Mycobacteriol*, DOI:10.1016/j.ijmyco.2016.03.004.

82 S. S. Hakkimane, V. P. Shenoy, S. L. Gaonkar, I. Bairy and B. R. Guru, *Int J Nanomedicine*, 2018, **13**, 4303–4318.

83 M. Getahun, H. M. Blumberg, G. Ameni, D. Beyene and R. R. Kempker, *PLoS One*, 2022, **17**, e0274426.

84 F. B. Perler, *Nucleic Acids Res*, DOI:10.1093/nar/30.1.383.

85 M. Qiao, W. Ren, H. Guo, F. Huo, Y. Shang, Y. Wang, M. Gao and Y. Pang, *International Journal of Infectious Diseases*, 2021, **106**, 295–299.

86 L. D. Forsman, K. Niward, J. Kuhlin, X. Zheng, R. Zheng, R. Ke, C. Hong, J. Werngren, J. Paues, U. S. H. Simonsson, E. Eliasson, S. Hoffner, B. Xu, J. W. Alffenaar, T. Schön, Y. Hu and J. Bruchfeld, *European Respiratory Journal*, 2021, **57**, 2003463.

87 K. A. Ängeby, P. Jureen, C. G. Giske, E. Chryssanthou, E. Sturegård, M. Nordvall, A. G. Johansson, J. Werngren, G. Kahlmeter, S. E. Hoffner and T. Schön, *Journal of Antimicrobial Chemotherapy*, 2010, **65**, 946–952.

88 N. Kumari, R. Sharma, J. Ali, G. Chandra, S. Singh and M. Y. Krishnan, *Tuberculosis*, DOI:10.1016/j.tube.2024.102479.

89 M. T. Heinrichs, R. J. May, F. Heider, T. Reimers, S. K. B. Sy, C. A. Peloquin and H. Derendorf, *Int J Mycobacteriol*, DOI:10.4103/ijmy.ijmy_33_18.

90 J. E. M. De Steenwinkel, R. E. Aarnoutse, G. J. De Knegt, M. T. Ten Kate, M. Teulen, H. A. Verbrugh, M. J. Boeree, D. Van Soolingen and I. A. J. M. Bakker-Woudenberg, *Am J Respir Crit Care Med*, DOI:10.1164/rccm.201207-1210OC.

91 I. M. Rosenthal, R. Tasneen, C. A. Peloquin, M. Zhang, D. Almeida, K. E. Mdluli, P. C. Karakousis, J. H. Grosset and E. L. Nuermberger, *Antimicrob Agents Chemother*, DOI:10.1128/AAC.00912-12.

92 B. Pottakkat, A. Kumar, A. Rastogi, N. Krishnani, V. K. Kapoor and R. Saxena, *Gut Liver*, DOI:10.5009/gnl.2010.4.1.94.

93 D. A. Lestari, N. Rahadiani and R. A. Syaiful, *Int J Surg Case Rep*, DOI:10.1016/j.ijscr.2021.105966.

94 Y. Tojo, S. Yanagisawa, E. Miyauchi and M. Ichinose, *International Journal of Infectious Diseases*, 2018, 67.

95 L. Kremer, J. Estaquier, I. Wolowczuk, F. Biet, J. C. Ameisen and C. Locht, *Infect Immun*, DOI:10.1128/IAI.68.7.4264-4273.2000.

96 A. Masumi, K. Mochida, K. Takizawa, T. Mizukami, M. Kuramitsu, M. Tsuruhara, S. Mori, K. Shibayama, K. Yamaguchi and I. Hamaguchi, *Inflamm Regen*, DOI:10.1186/s41232-016-0024-3.

97 A. Nava, A. C. Hahn, T. H. Wu and T. F. Byrd, *Front Immunol*, DOI:10.3389/fimmu.2022.1017540.

98 S. M. Lewis, A. Williams and S. C. Eisenbarth, *Sci Immunol*, 2019, 4.

99 B. S. Steiniger, *Immunology*, DOI:10.1111/imm.12469.

100 S. M. Szczepanek, J. T. McNamara, E. R. Secor, P. Natarajan, L. A. Guernsey, L. A. Miller, E. Ballesteros, E. Jellison, R. S. Thrall and B. Andemariam, *American Journal of Pathology*, DOI:10.1016/j.ajpath.2012.07.034.

101 W. Wehrli, *Rev Infect Dis*, DOI:10.1093/clinids/5.Supplement_3.S407.

102 United Nations, The Sustainable Development Goals Report 2023, https://unstats.un.org/sdgs/report/2023/, (accessed 2 July 2024).

103 H. Paulus, *Frontiers in Bioscience-Landmark*, 2003, **8**, 1157–1165.

104 R. Álvarez-Chimal and J. Ángel Arenas-Alatorre, in *Green Chemistry for Environmental Sustainability - Prevention-Assurance-Sustainability (P-A-S) Approach*, 2023.

105 J. Iqbal, B. A. Abbasi, T. Yaseen, S. A. Zahra, A. Shahbaz, S. A. Shah, S. Uddin, X. Ma, B. Raouf, S. Kanwal, W. Amin, T. Mahmood, H. A. El-Serehy and P. Ahmad, *Sci Rep*, DOI:10.1038/s41598-021-99839-z.

A.

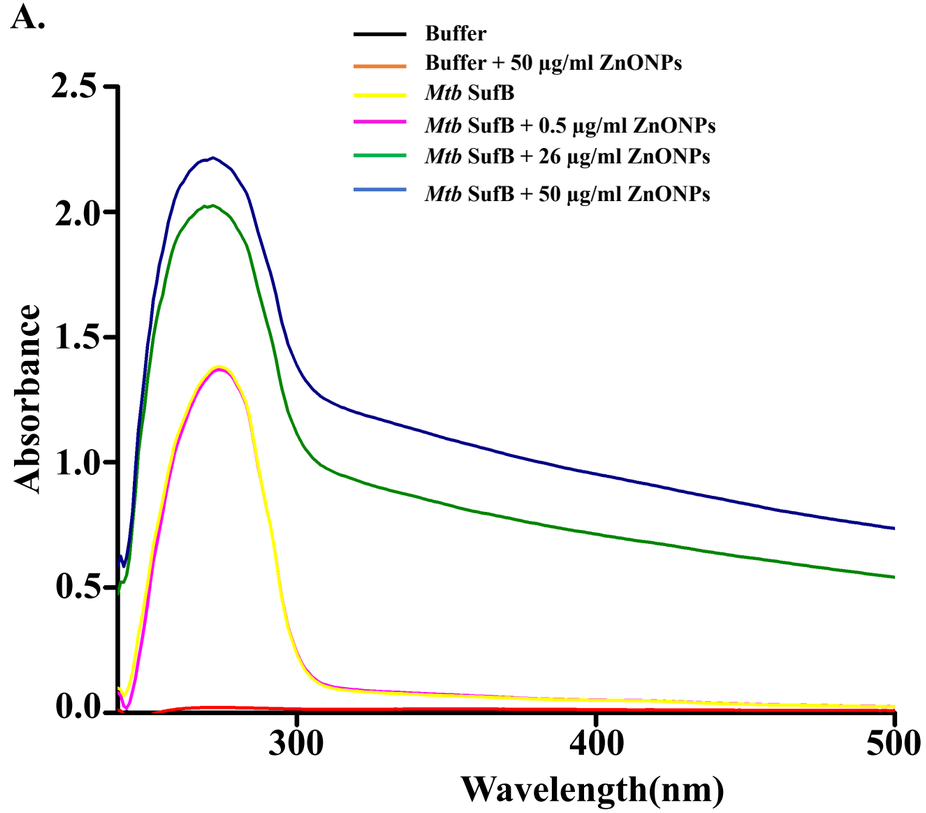

B.

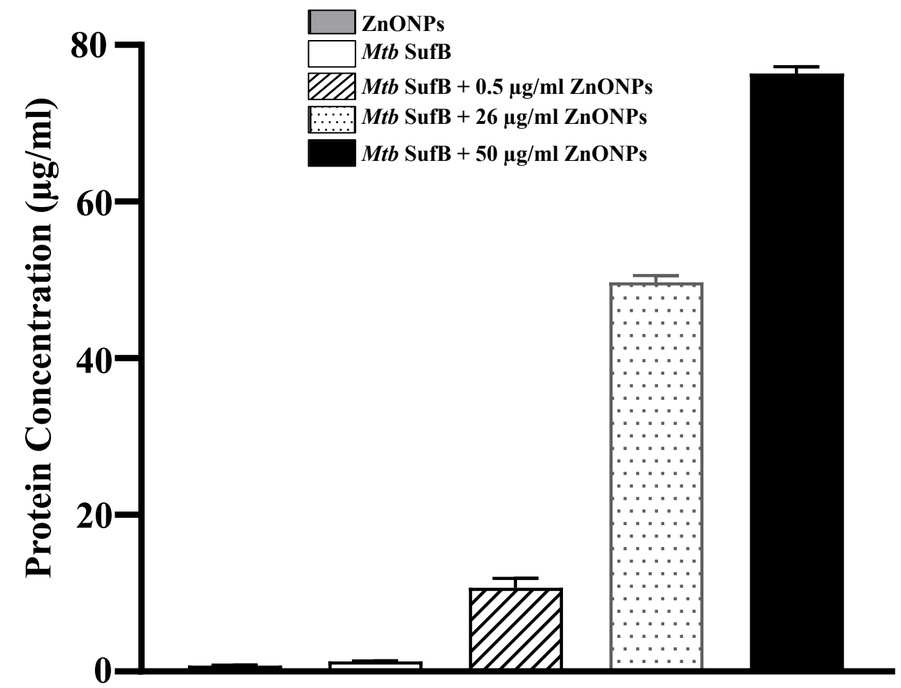

C.

i)

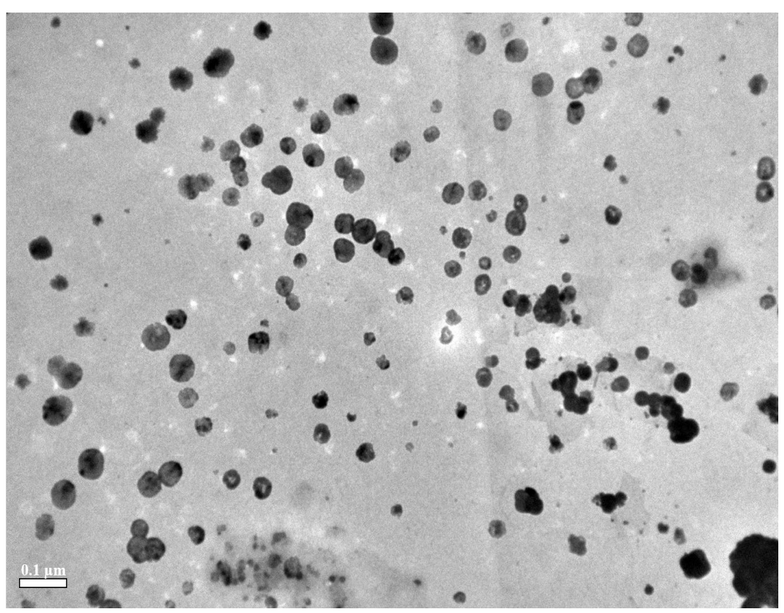

ZnONP

ii)

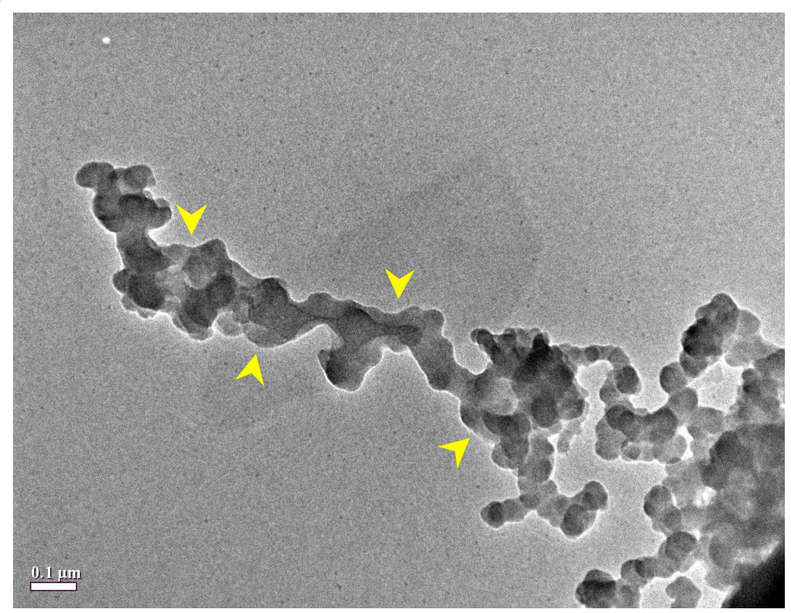

iii)

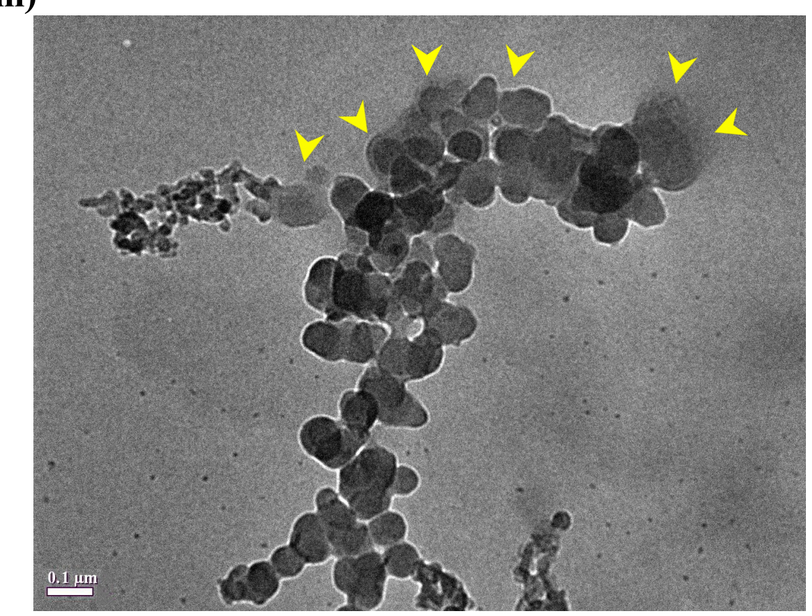

Mtu SufB + 50 µg/ml ZnONP

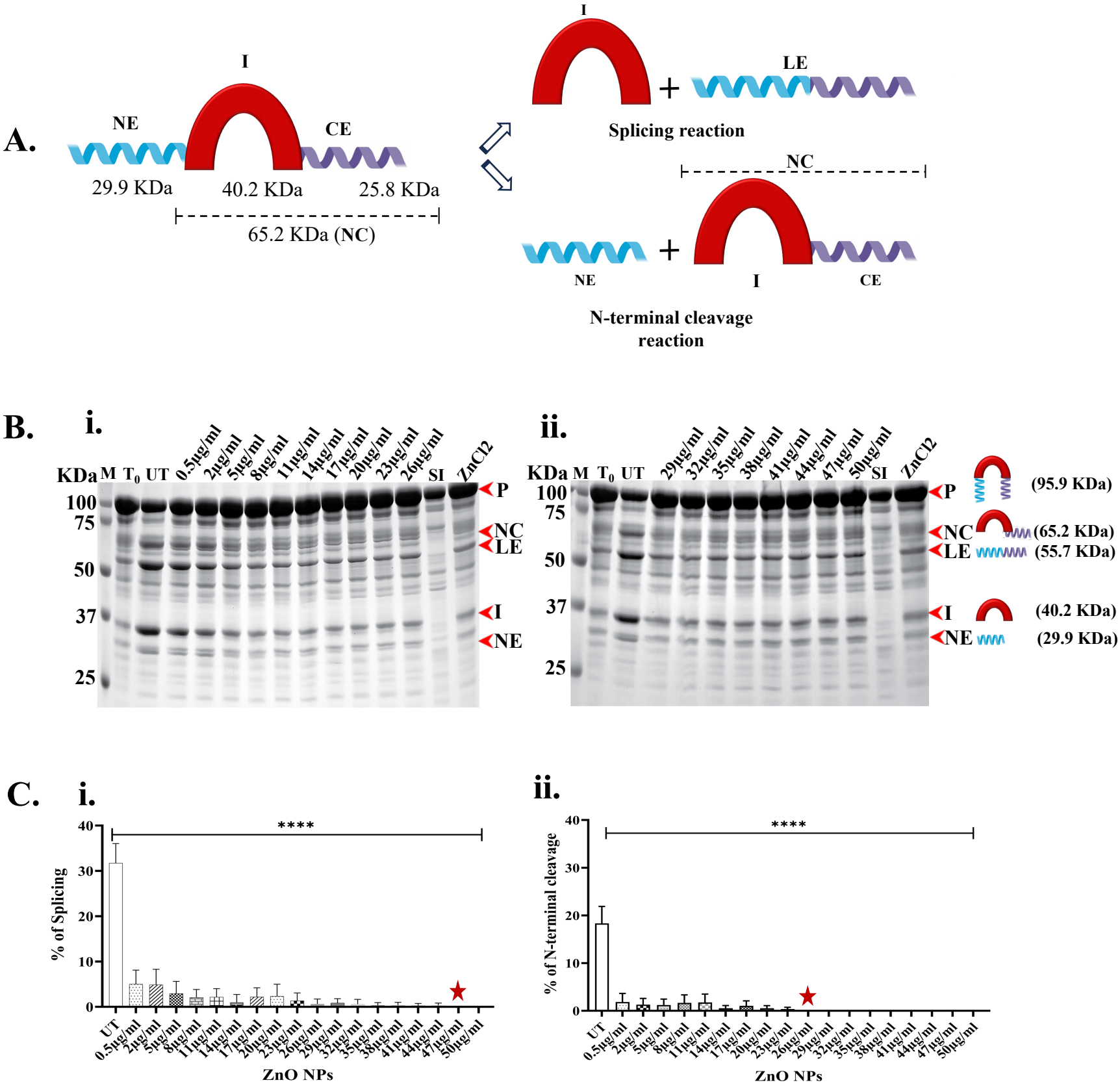
A.
I
NE
CE
29.9 KDa
40.2 KDa
25.8 KDa
65.2 KDa (NC)
I
LE
Splicing reaction
NC
NE
I
CE
N-terminal cleavage reaction
B.
i.
KDa M T0 UT 0.5µg/ml 2µg/ml 5µg/ml 8µg/ml 11µg/ml 14µg/ml 17µg/ml 20µg/ml 23µg/ml 26µg/ml SI ZnCl2
100
75
50
37
25
P
NC
LE
I
NE
ii.
KDa M T0 UT 29µg/ml 32µg/ml 35µg/ml 38µg/ml 41µg/ml 44µg/ml 47µg/ml 50µg/ml SI ZnCl2
100
75
50
37
25
P (95.9 KDa)
NC (65.2 KDa)
LE (55.7 KDa)
I (40.2 KDa)
NE (29.9 KDa)
C.
i.
% of Splicing
****
UT
0.5µg/ml
2µg/ml
5µg/ml
8µg/ml
11µg/ml
14µg/ml
17µg/ml
20µg/ml
23µg/ml
26µg/ml
29µg/ml
32µg/ml
35µg/ml
38µg/ml
41µg/ml
44µg/ml
47µg/ml
50µg/ml
ZnO NPs
ii.
% of N-terminal cleavage
****
ZnO NPs

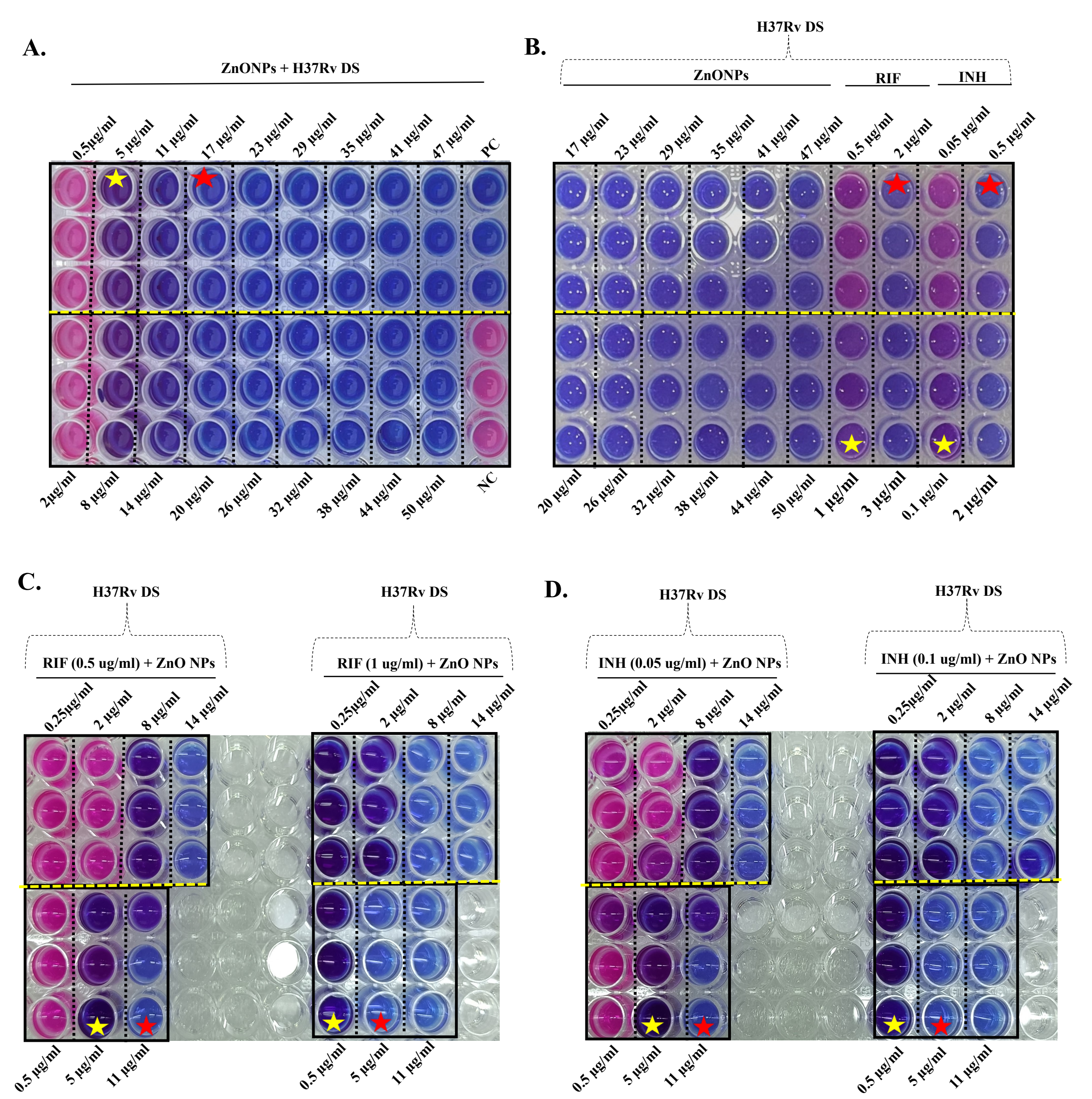
A.
ZnONPs + H37Rv DS
0.5µg/ml
5 µg/ml
11 µg/ml
17 µg/ml
23 µg/ml
29 µg/ml
35 µg/ml
41 µg/ml
47 µg/ml
PC
2µg/ml
8 µg/ml
14 µg/ml
20 µg/ml
26 µg/ml
32 µg/ml
38 µg/ml
44 µg/ml
50 µg/ml
NC
B.
H37Rv DS
ZnONPs
RIF
INH
17 µg/ml
23 µg/ml
29 µg/ml
35 µg/ml
41 µg/ml
47 µg/ml
0.5 µg/ml
2 µg/ml
0.05 µg/ml
0.5 µg/ml
20 µg/ml
26 µg/ml
32 µg/ml
38 µg/ml
44 µg/ml
50 µg/ml
1 µg/ml
3 µg/ml
0.1 µg/ml
2 µg/ml
C.
H37Rv DS
RIF (0.5 ug/ml) + ZnO NPs
0.25µg/ml
2 µg/ml
8 µg/ml
14 µg/ml
0.5 µg/ml
5 µg/ml
11 µg/ml
H37Rv DS
RIF (1 ug/ml) + ZnO NPs
0.25µg/ml
2 µg/ml
8 µg/ml
14 µg/ml
0.5 µg/ml
5 µg/ml
11 µg/ml
D.
H37Rv DS
INH (0.05 ug/ml) + ZnO NPs
0.25µg/ml
2 µg/ml
8 µg/ml
14 µg/ml
0.5 µg/ml
5 µg/ml
11 µg/ml
H37Rv DS
INH (0.1 ug/ml) + ZnO NPs
0.25µg/ml
2 µg/ml
8 µg/ml
14 µg/ml
0.5 µg/ml
5 µg/ml
11 µg/ml

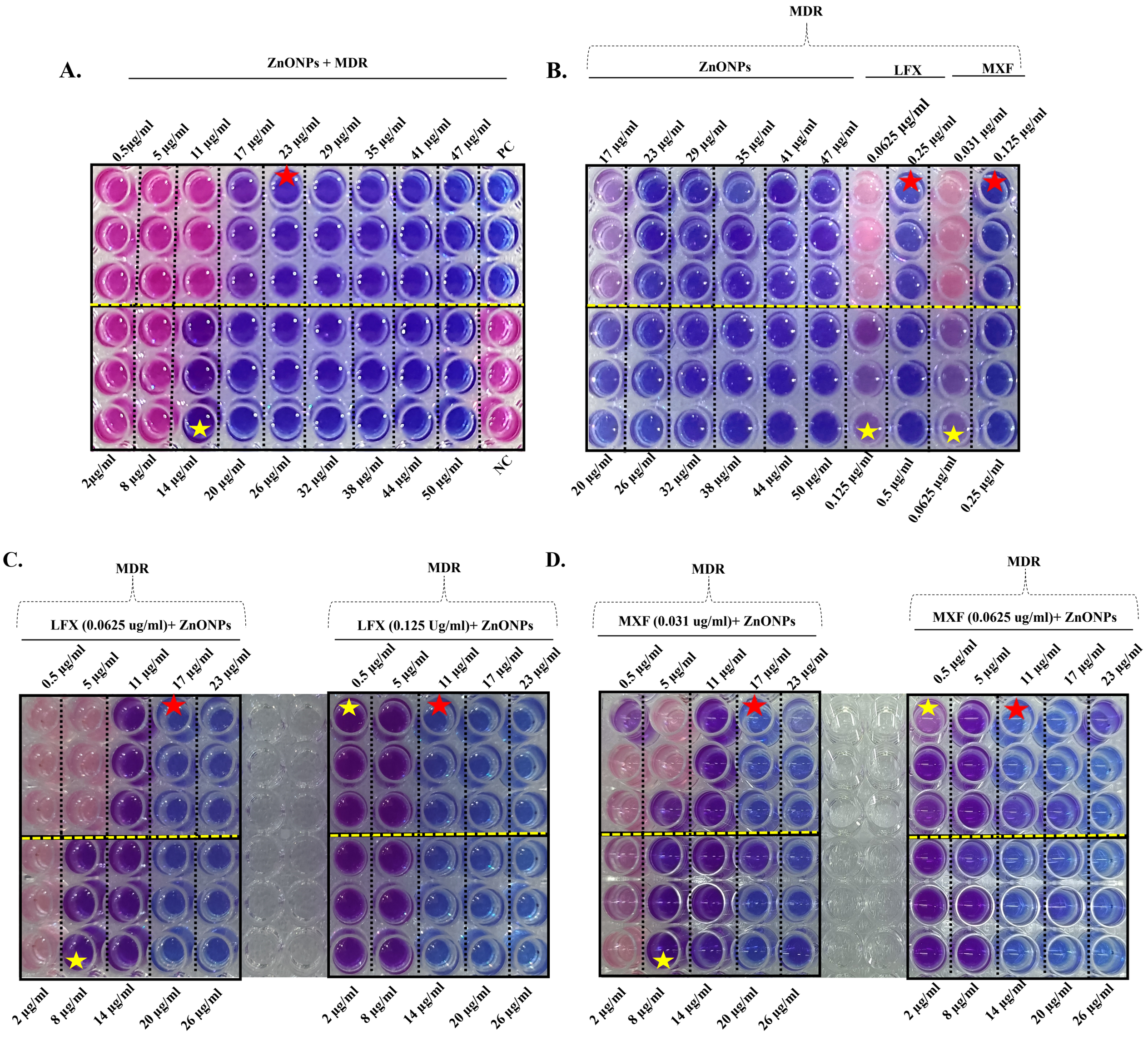
A.
ZnONPs + MDR
0.5µg/ml
5 µg/ml
11 µg/ml
17 µg/ml
23 µg/ml
29 µg/ml
35 µg/ml
41 µg/ml
47 µg/ml
PC
2µg/ml
8 µg/ml
14 µg/ml
20 µg/ml
26 µg/ml
32 µg/ml
38 µg/ml
44 µg/ml
50 µg/ml
NC
B.
MDR
ZnONPs
LFX
MXF
17 µg/ml
23 µg/ml
29 µg/ml
35 µg/ml
41 µg/ml
47 µg/ml
0.0625 µg/ml
0.25 µg/ml
0.031 µg/ml
0.125 µg/ml
20 µg/ml
26 µg/ml
32 µg/ml
38 µg/ml
44 µg/ml
50 µg/ml
0.125 µg/ml
0.5 µg/ml
0625 µg/ml
0.25 µg/ml
C.
MDR
LFX (0.0625 ug/ml)+ ZnONPs
0.5 µg/ml
5 µg/ml
11 µg/ml
17 µg/ml
23 µg/ml
2 µg/ml
8 µg/ml
14 µg/ml
20 µg/ml
26 µg/ml
MDR
LFX (0.125 Ug/ml)+ ZnONPs
0.5 µg/ml
5 µg/ml
11 µg/ml
17 µg/ml
23 µg/ml
2 µg/ml
8 µg/ml
14 µg/ml
20 µg/ml
26 µg/ml
D.
MDR
MXF (0.031 ug/ml)+ ZnONPs
0.5 µg/ml
5 µg/ml
11 µg/ml
17 µg/ml
23 µg/ml
2 µg/ml
8 µg/ml
14 µg/ml
20 µg/ml
26 µg/ml
MDR
MXF (0.0625 ug/ml)+ ZnONPs
0.5 µg/ml
5 µg/ml
11 µg/ml
17 µg/ml
23 µg/ml
2 µg/ml
8 µg/ml
14 µg/ml
20 µg/ml
26 µg/ml

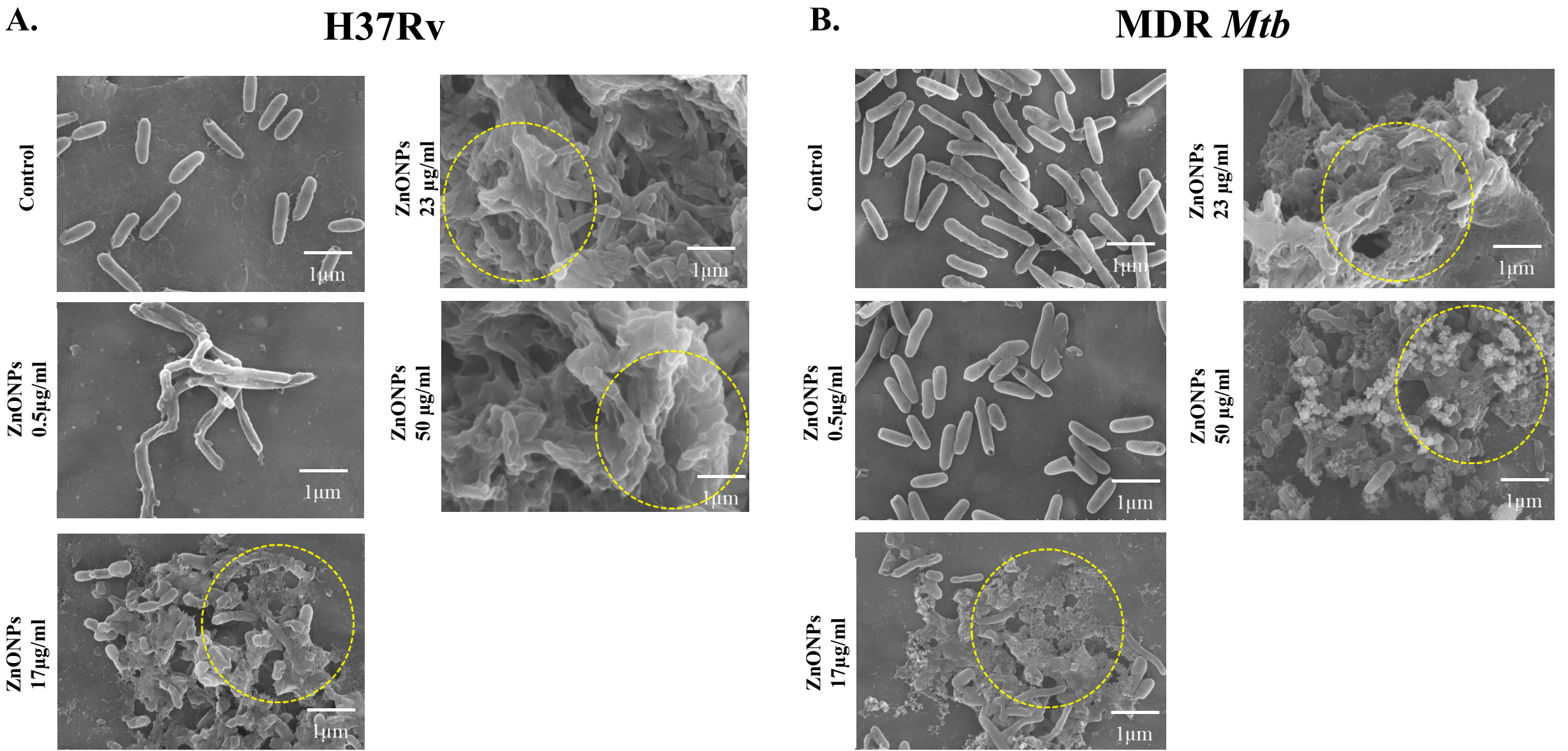
A.
H37Rv
Control
ZnONPs 23 µg/ml
ZnONPs 0.5µg/ml
ZnONPs 50 µg/ml
ZnONPs 17µg/ml
1µm
B.
MDR *Mtb*
Control
ZnONPs 23 µg/ml
ZnONPs 0.5µg/ml
ZnONPs 50 µg/ml
ZnONPs 17µg/ml
1µm

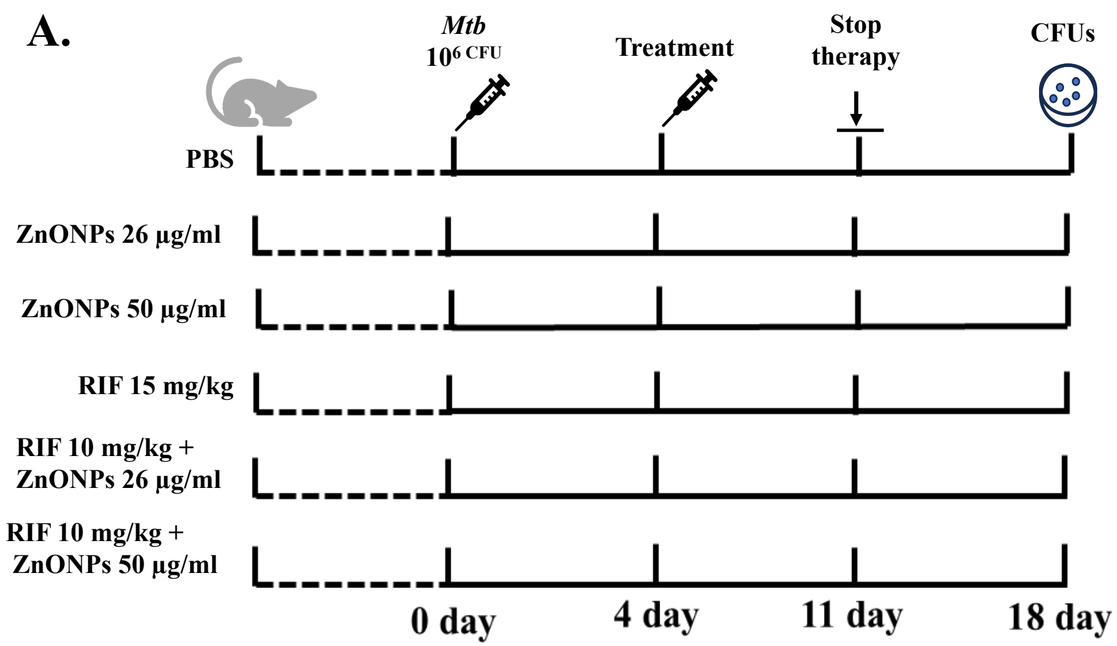
A.
Mtb
10⁶ CFU
Treatment
Stop therapy
CFUs
PBS
ZnONPs 26 µg/ml
ZnONPs 50 µg/ml
RIF 15 mg/kg
RIF 10 mg/kg + ZnONPs 26 µg/ml
RIF 10 mg/kg + ZnONPs 50 µg/ml
0 day
4 day
11 day
18 day

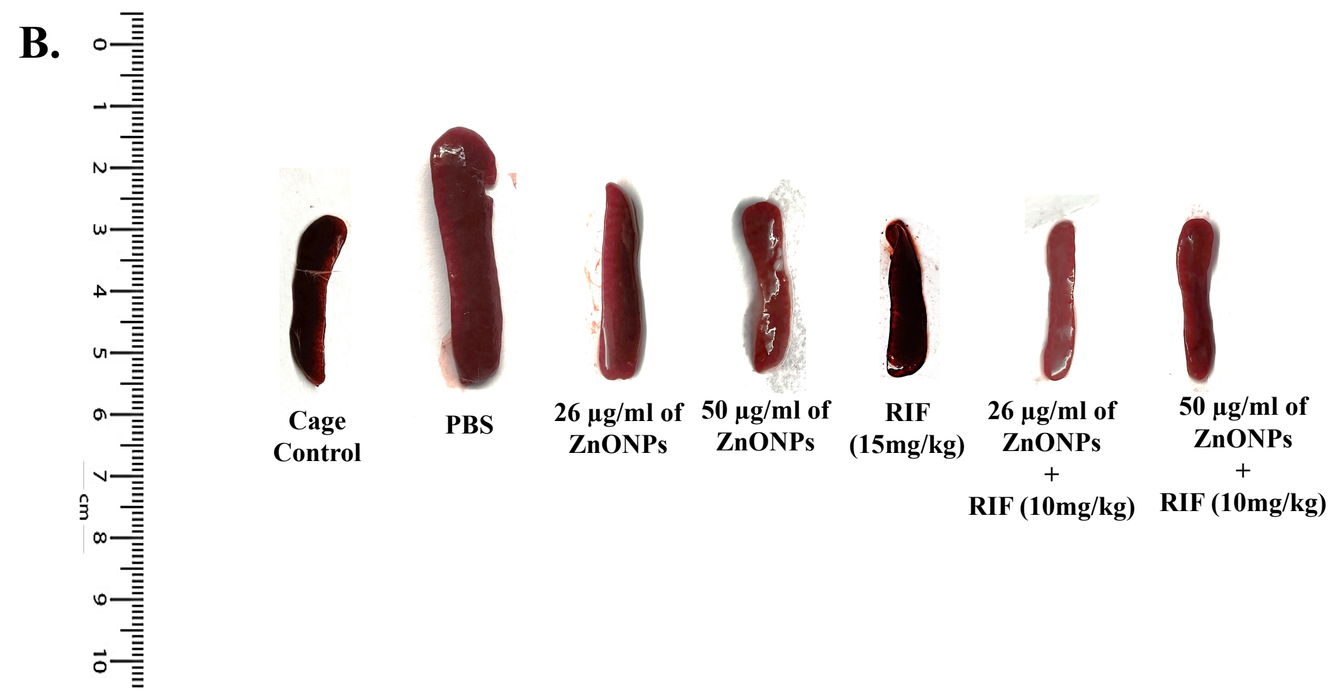
B.
Cage Control
PBS
26 µg/ml of ZnONPs
50 µg/ml of ZnONPs
RIF (15mg/kg)
26 µg/ml of ZnONPs + RIF (10mg/kg)
50 µg/ml of ZnONPs + RIF (10mg/kg)

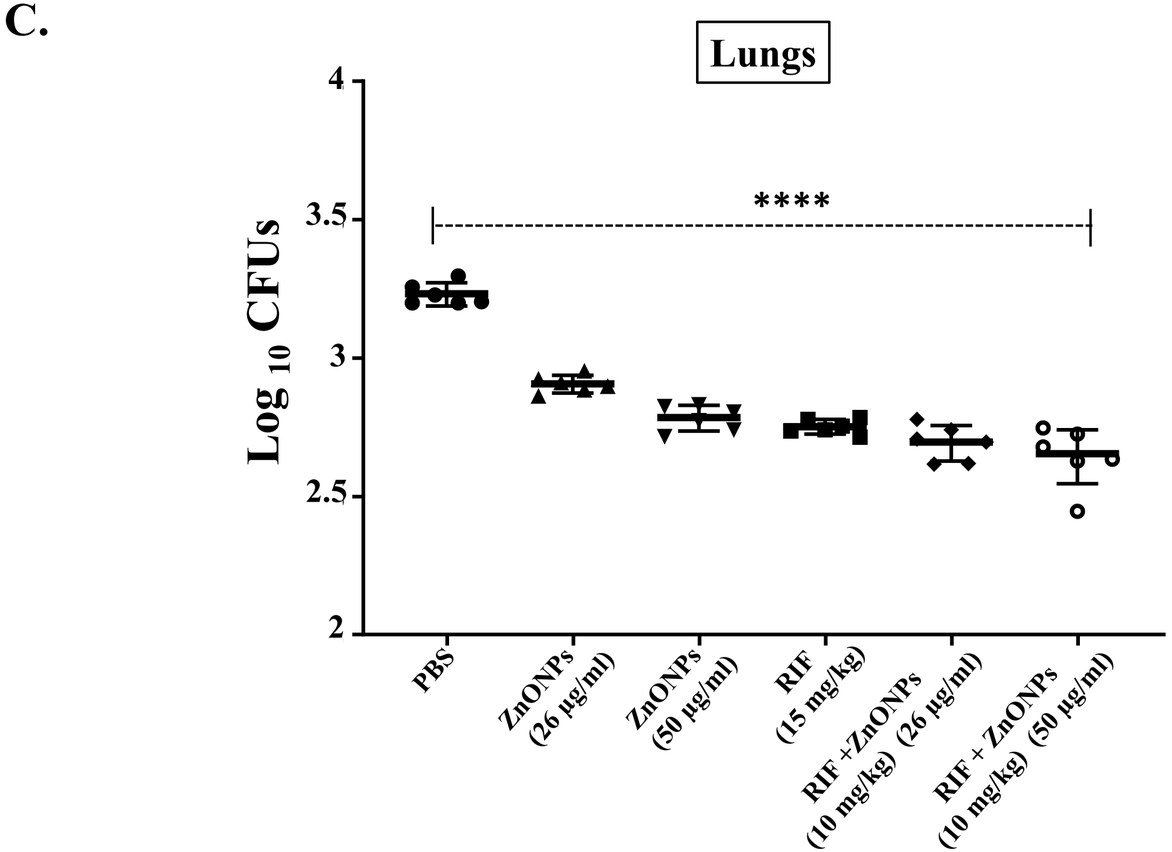
C.
Lungs
Log 10 CFUs
****
PBS
ZnONPs (26 µg/ml)
ZnONPs (50 µg/ml)
RIF (15 mg/kg)
RIF +ZnONPs (10 mg/kg) (26 µg/ml)
RIF + ZnONPs (10 mg/kg) (50 µg/ml)

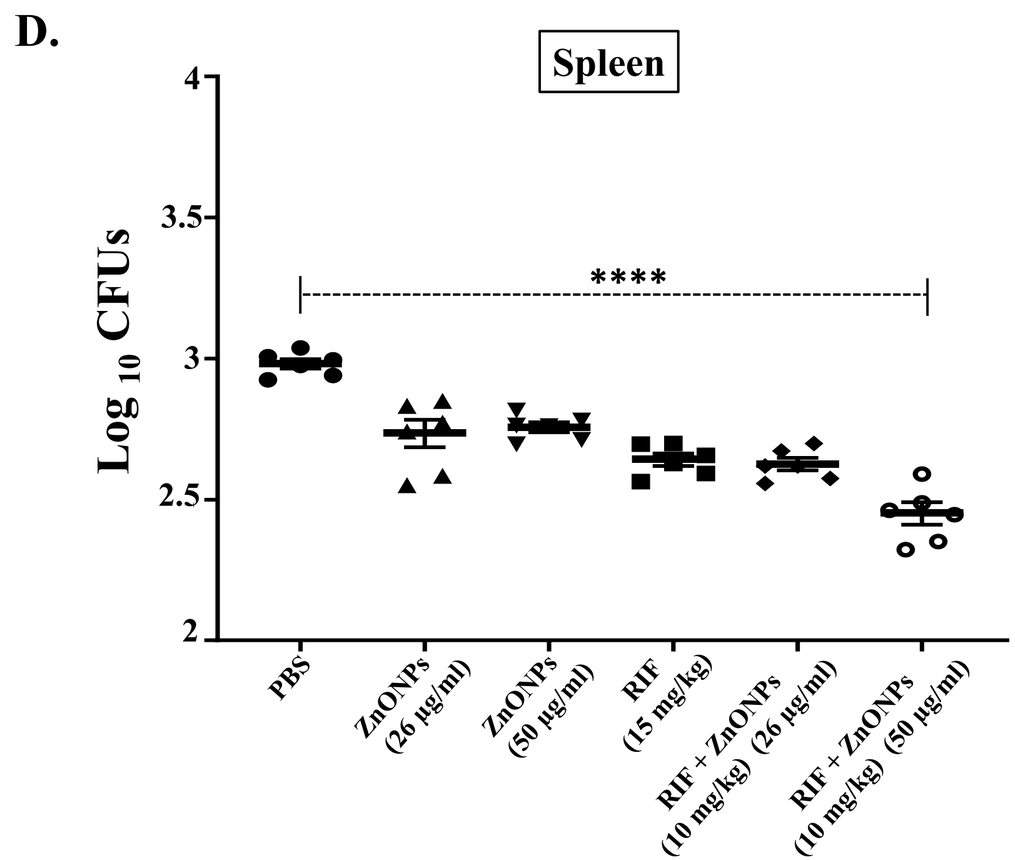
D.
Spleen
Log 10 CFUs
****
PBS
ZnONPs (26 µg/ml)
ZnONPs (50 µg/ml)
RIF (15 mg/kg)
RIF + ZnONPs (10 mg/kg) (26 µg/ml)
RIF + ZnONPs (10 mg/kg) (50 µg/ml)

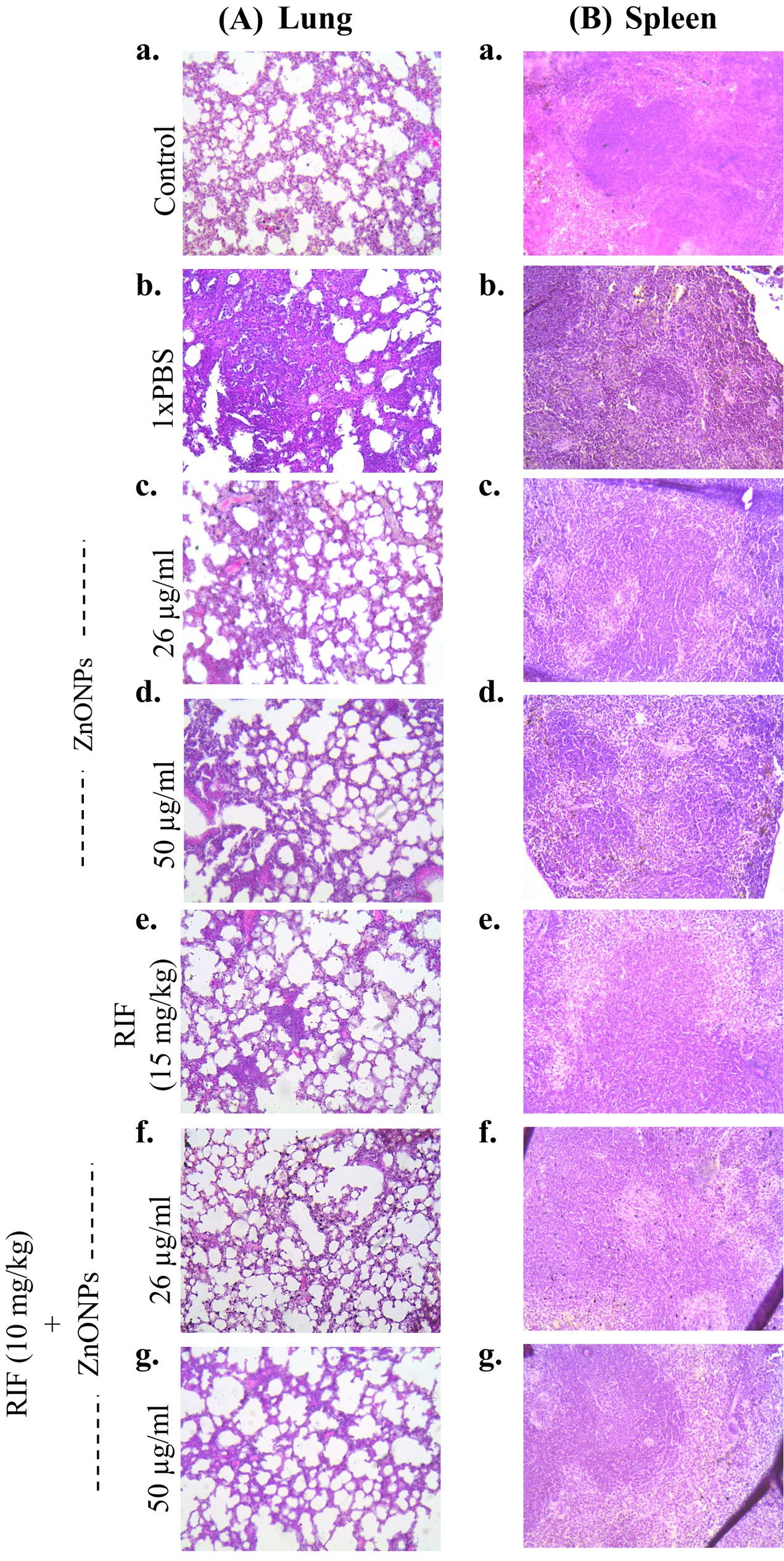
(A) Lung
(B) Spleen
a.
Control
b.
1xPBS
c.
26 µg/ml
d.
50 µg/ml
ZnONPs
e.
RIF
(15 mg/kg)
f.
26 µg/ml
g.
50 µg/ml
RIF (10 mg/kg)
+
ZnONPs

Conventional anti-TB drug therapy (Drug-sensitive and MDR *Mtb* strains)

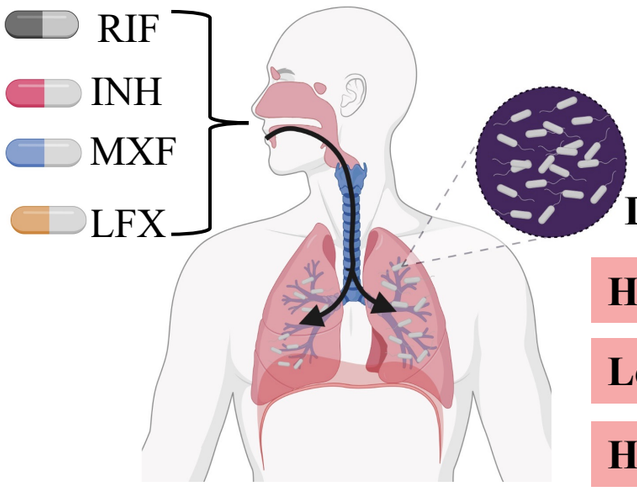

Dead Bacteria

- **High dose**
- **Longer duration of therapy**
- **High toxicity**
- **Patient non-compliance**

ZnONP-based combinatorial anti-TB drug therapy (Drug-sensitive and MDR *Mtb* strains)

ZnO NPs

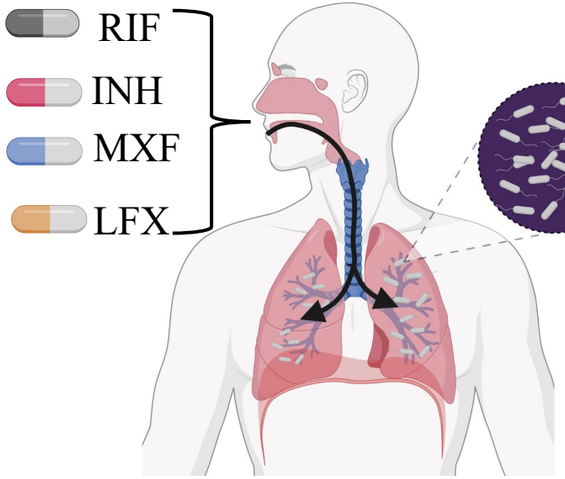

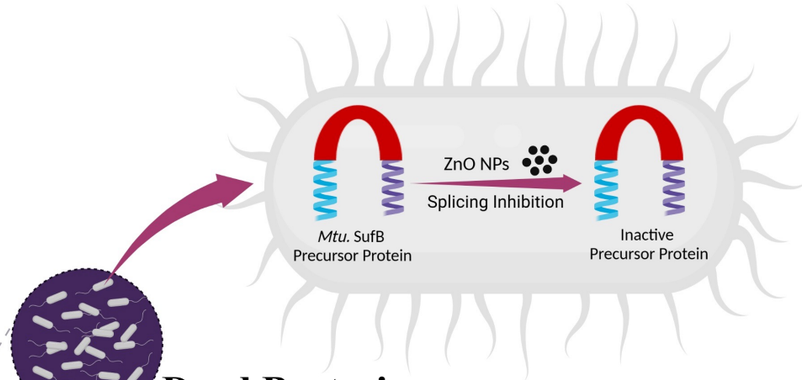

Dead Bacteria

- **Low dose**
- **Shorter duration of therapy**
- **Low toxicity**
- **Better patient compliance**